www.czasopisma.pan.pl PAN POLSKA AKADEMIA NAUK www.journals.pan.pl

Acta Geologica Polonica, Vol. 70 (2020), No. 1, pp. 1–29
DOI: 10.24425/agp.2019.126454

Fluid pathways within shallow-generated damage zones of strike-slip faults – evidence of map-scale faulting in a continental environment, SW Permo-Mesozoic cover of the Late Palaeozoic Holy Cross Mountains Fold Belt, Poland

BARBARA RYBAK-OSTROWSKA[1]*, ANDRZEJ KONON[1], VRATISLAV HURAI[2], MACIEJ BOJANOWSKI[3], AGNIESZKA KONON[4], and MICHAŁ WYGLĄDAŁA[1]

[1] *University of Warsaw, Faculty of Geology, Żwirki i Wigury 93, 02-089 Warsaw, Poland.*
[2] *Slovak Academy of Sciences, Earth Science Institute, Dúbravská cesta 9, 840 05 Bratislava, Slovakia.*
[3] *Polish Academy of Sciences, Institute of Geological Sciences, Twarda 51/55, 00-818 Warsaw, Poland.*
[4] *Polish Geological Institute – National Research Institute, Rakowiecka 4, 00-975 Warsaw, Poland.*
* *Corresponding author: barbara.rybak@uw.edu.pl*

ABSTRACT:

Rybak-Ostrowska, B., Konon, A., Hurai, V., Bojanowski, M., Konon, A. and Wyglądała, M. 2020. Fluid pathways within shallow-generated damage zones of strike-slip faults – evidence of map-scale faulting in a continental environment, SW Permo-Mesozoic cover of the Late Palaeozoic Holy Cross Mountains Fold Belt, Poland. *Acta Geologica Polonica*, **70** (1), 1–29. Warszawa.

The damage zones of exhumed strike-slip faults dissecting Jurassic carbonates in the south-western part of the Late Palaeozoic Holy Cross Mountains Fold Belt reveal second-order faults and fractures infilled with syntectonic calcite. The subsequent development of a structural pattern of microscopic fault-related structures and calcite infillings reflects the activity of strike-slip faults that began in the Late Cretaceous (Late Maastrichtian) and lasted until the early Miocene (Langhian). The fabric of the syntectonic veins provides insights into the evolution of the permeable fault-related structures that were the main pathways for fluid flow during fault activity. Microstructural study of calcite veins coupled with stable isotope and fluid inclusion data indicates that calcite precipitated primarily in a rock-buffered system related to strike-slip fault movement, and secondarily in a partly open system related to the local activity of the releasing Chmielnik stepover or the uplift of the area. The presence of meteoric fluids descending from the surface into damage zones suggest that the strike-slip faulting might have taken place in a nonmarine, continental environment.

Key words: Strike-slip faulting; Fluid pathways; Continental environment; Chmielnik releasing stepover; Permo-Mesozoic cover; Holy Cross Mountains Fold Belt.

INTRODUCTION

The formation of strike-slip fault associated structures is widely recognised in all environments from abyssal to continental (e.g., Reading 1980; Ben-Avraham 1985; Sylvester 1988; Woodcock and Schubert 1994; Wakabayashi *et al*. 2004; Wakabayashi 2007). Passively exhumed strike-slip fault zones display an internal structure with highly damaged cores at considerable depth and broad damage zones in the top few kilometres of the crust (Finzi *et al.* 2009). The fault zones are common fluid pathways, although their heterogeneous architecture constrains the flow in space and time (Chester *et al.* 1993;

Knipe 1993; Caine *et al.* 1996). The fault cores accommodate displacement and comprise individual surfaces or fault rocks that can be conduits or barriers for fluids (Chester and Logan 1986; Caine *et al.* 1996; Sibson 1996, 2000; Billi *et al.* 2003; Faulkner *et al.* 2003; Wibberley *et al.* 2008). Damage zones reveal a subsidiary fault and fracture network with a potential for fluid transport during deformation (Chester and Logan 1986; Cain *et al.* 1996, 1999; Faulkner *et al.* 2003; Wibberley and Shimamoto 2003; Micklethwaite and Cox 2004; Brogi 2008; Zhang *et al.* 2008; Kim and Sanderson 2010). The damage of rocks during faulting is often associated with fluids of meteoric origin descending from the surface or fluids of magmatic or metamorphic origin ascending from deep-crustal parts of the seismogenic zone (e.g., Oliver 1996; Pili *et al.* 2002; Agosta and Kirschner 2003; Cox 2007; Fitz-Diaz *et al.* 2011; Cao and Neubauer 2016). When faulting involves carbonate rocks, pressure solution affects fault zones and local mass transfer occurs (e.g., Marshak *et al.* 1982; Kim *et al.* 2003; Agosta and Aydi 2006; Gratier *et al.* 2013). Consequently, fluid presence and pressure solution of rocks enhance the sealing of the subsidiary fault and fracture network within damage zones. Thus, the relationship between faulting/fracturing and mineral infilling is recorded by syntectonic mineral growth (Durney and Ramsay 1973; Passchier and Trouw 1996) within extensional mode I, shear mode II and III or hybrid structures of modes I and II or III (e.g., Pollard and Segall 1987; Engelder 1999; Scholz 2002; Ramsay and Chester 2004).

The aim of this paper is to describe the evolution of the top 1–2 km of strike-slip fault zones dissecting the south-western part of both the Permo-Mesozoic cover of the Late Palaeozoic Holy Cross Mountains Fold Belt (HCFB) and the Cenozoic rocks belonging to the Carpathian Foredeep Basin in relation to the exhumation processes (Text-fig. 1). The damage zones of the strike-slip faults that developed within the Jurassic rocks consist of secondary minor faults and fractures (Konon and Mastella 2001; Mastella and Konon 2002; Konon 2015; Konon *et al.* 2016; Rybak-Ostrowska *et al.* 2017). We consider these second-order structures as pathways for fluids recorded by the syntectonic precipitation of calcite. The structural pattern of the microscopic fault-related structures and fabrics of syntectonic veins coupled with the stable isotope and fluid inclusion data of their calcite infilling provide insights into the fluid source and evolution of permeable structures during fault activity. The intense stress that induced the solution of rocks analysed in relation to the calcite sealing second-order faults and fractures gives hints on the dissolution and precipitation processes within the fault zones. The integration of all this assembled data has provided the basis for discussing the progressive development of the structural pattern within strike-slip fault zones and fluid transport in relation to the exhumation processes of the study area during Cretaceous–Cenozoic deformation stages.

GEOLOGICAL SETTING

The strike-slip fault pattern in the Permo-Mesozoic cover of the south-western part of the Late Palaeozoic Holy Cross Mountains Fold Belt (HCFB) consists of major N-S, NW-SE and NNW-SSE-striking faults, which connect with the WNW-ESE-striking faults near Małogoszcz town (Text-figs 1 and 2). The NW-SE and NNW-SSE-striking Mieczyn Fault connects in its southern part with the NW-SE and N-S-striking Snochowice Fault and with the WNW-ESE-striking Gnieździska-Brzeziny and Tokarnia faults. The Gnieździska-Brzeziny and Tokarnia faults propagate towards the south-east as the Staszów and Chmielnik faults, respectively. A prevailing dextral strike-slip movement component has been recognised along these faults (Konon and Mastella 2001; Mastella and Konon 2002; Konon 2015; Konon *et al.* 2016; Rybak-Ostrowska *et al.* 2017) (Text-fig. 2). The major faults merge and diverge along their strikes; as a result they form an anastomosing fault pattern. Locally, the subparallel strike-slip faults form stepovers, as for instance, the Mnin restraining stepover (Konon 2015; Konon *et al.* 2016; Text-figs 1, 2A–C).

The large scale strike-slip faulting within the south-western part of the Permo-Mesozoic cover of the HCFB has been associated with the Cretaceous/Palaeogene inversion of the Polish Basin (Pożaryski 1964; Kutek and Głazek 1972, Dadlez *et al.* 1997; Krzywiec 2000, 2002, 2007; Hakenberg and Świdrowska 2001; Świdrowska 2007; Świdrowska *et al.* 2008; Konon *et al.* 2016). This process was initiated during the Late Cretaceous as a result of collisional phases in the Alpine and Carpathian orogens, and additionally opening of the Atlantic (e.g., Ziegler 1987, 1990a, b; Golonka *et al.* 2000; Dadlez 2003; Mazur *et al.* 2005). The faults dissect Triassic, Jurassic and Cretaceous rocks of the Permo-Mesozoic cover of the HCFB. The rocks formed as epicratonic sediments reaching a thickness of 2–4 km. The lowermost part of the Triassic succession is built of clastic sediments: conglomerates, sandstones, mudstones and claystones (Senkowiczowa 1961; Kuleta and Zbroja 2006). The

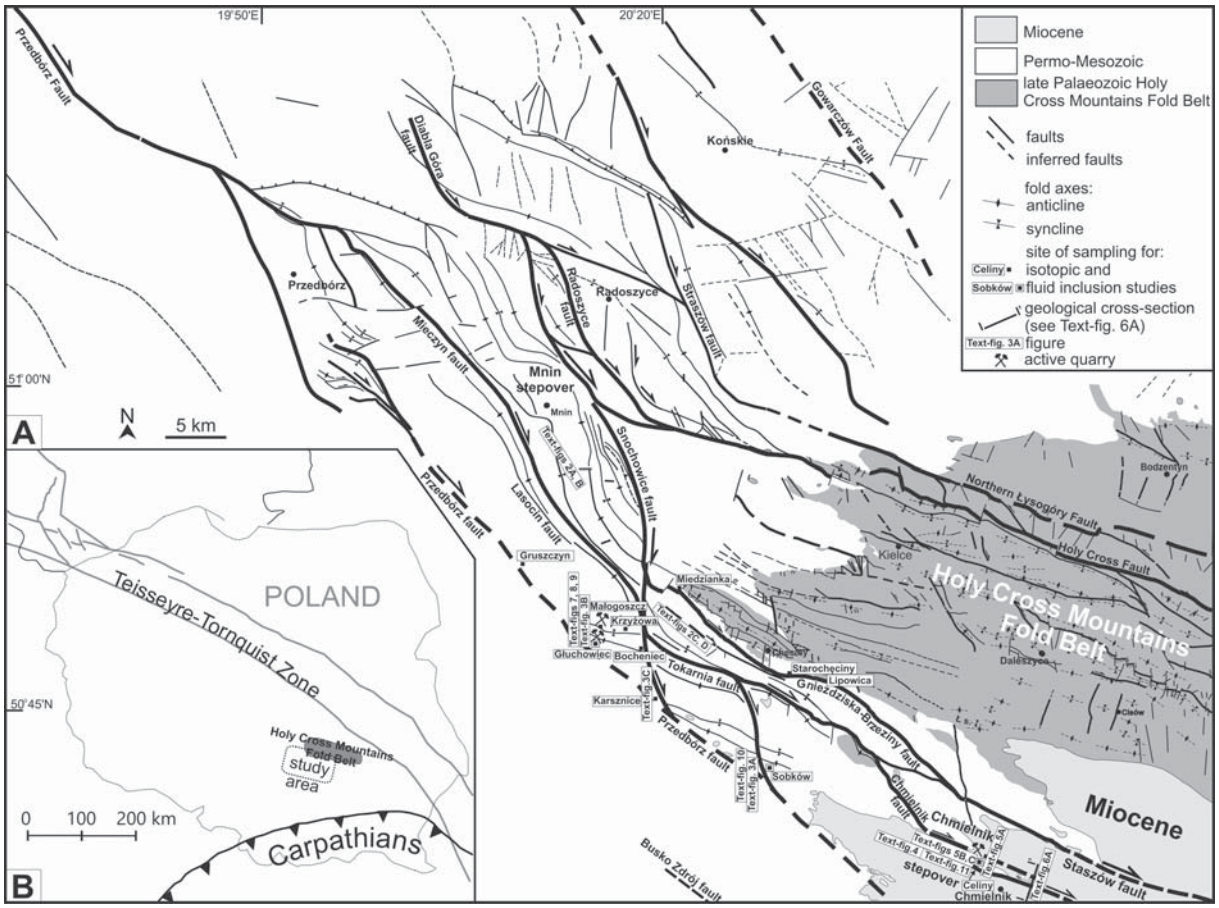

Text-fig. 1.Tectonic sketch-maps. A – Fault pattern within the Permo-Mesozoic cover in the western part of the Late Palaeozoic Holy Cross Mountains Fold Belt, Poland (based on Czarnocki 1938, 1961; Jurkiewiczowa 1961; Krajewski 1961; Różycki 1961; Jurkiewicz 1965, 1967; Filonowicz 1967; Grzybowski and Kutek 1967; Hakenberg 1973; Szajn 1977, 1980, 1983; Kwapisz 1983; Filonowicz and Lindner 1986; Cieśla and Lindner 1990; Janiec 1991; Mastella and Konon 2002; Konon 2007, 2015; Konon *et al.* 2016, modified). B – Location of the study area

Lower Triassic rocks are overlain by Middle Triassic limestones, dolomites, marls and claystones. The Upper Triassic sequence comprises claystones and mudstones with intercalations of sandstones, marls, dolomites, anhydrites and gypsum (Szajn 1984). The Lower Jurassic sequence is represented largely by terrestrial clastic rocks such as conglomerates and sandstones (Pieńkowski 1991, 2004; Świdrowska *et al*. 2008). The Middle Jurassic strata are composed of clastic marine sediments, such as clays, sandstones, siltstones and limestones (Matyja 2012). The Upper Jurassic rocks comprise Oxfordian and Kimmeridgian limestones and clayey marls (e.g., Kutek 1968; Matyja 1977; Matyja *et al*. 1996). The Upper Jurassic rocks are overlain by Lower Cretaceous sandstones, calcareous sandstones and spongiolites. The Upper Cretaceous rocks consist of limestones, sandstones and conglomerates, clays, siliceous limestones, marls and calcareous sandstones of Turonian to Maastrichtian ages (Marcinowski and Radwański 1983).

In the south-eastern part of the study area, near Chmielnik town, the Palaeozoic rocks of the HCFB and Mesozoic rocks are unconformably overlain by the transgressive Miocene sediments of the Carpathian Foredeep Basin (Radwański 1969, 1973; Radwański and Górka 2012; Górka 2015).

METHODS

Structural analysis

The structural observations were made along the Przedbórz, Snochowice, Gnieździska-Brzeziny

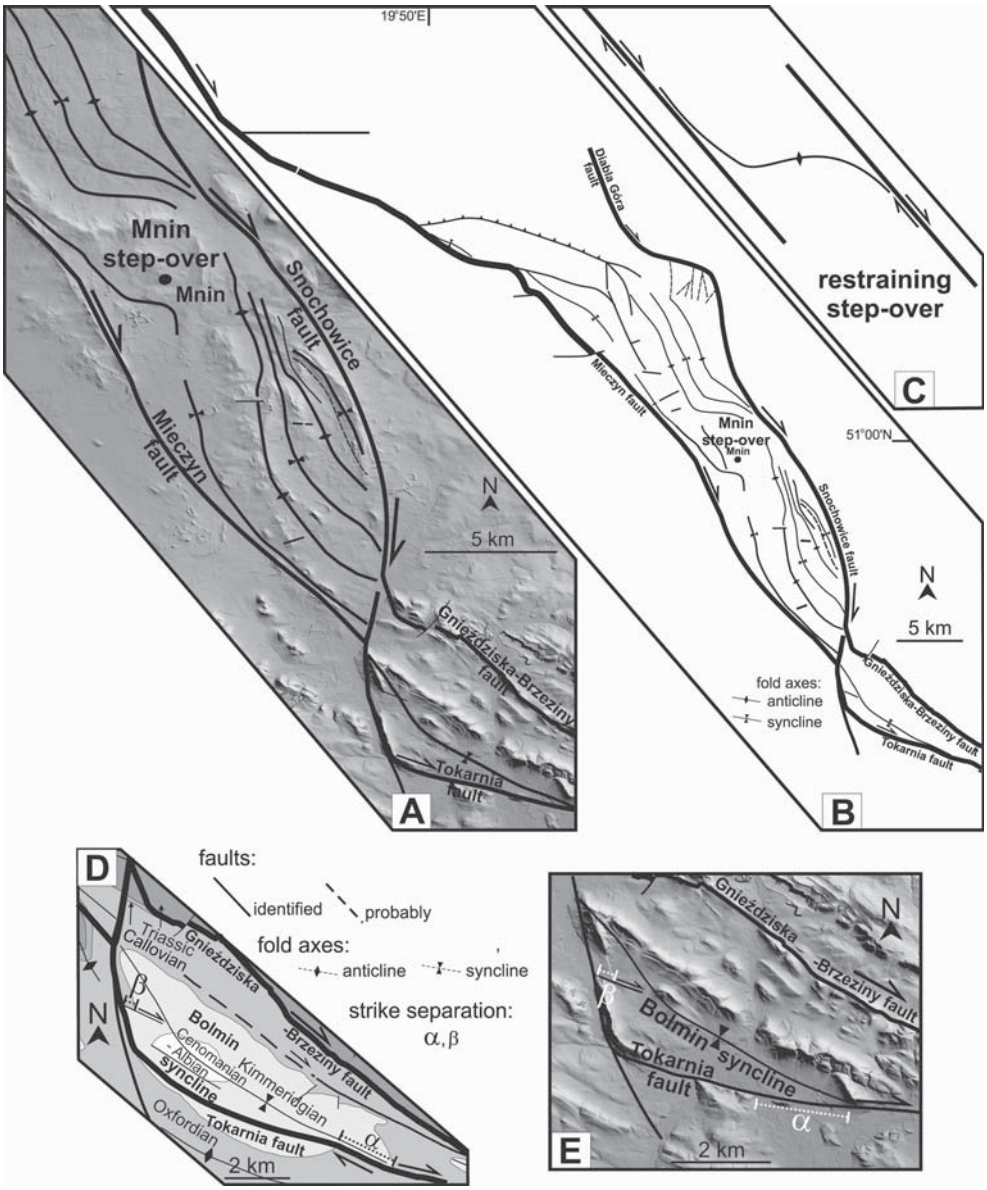

Text-fig. 2. Evidence of dextral strike-slip faulting within Permo-Mesozoic cover. A – Simplified tectonic map of the central part of the Mnin stepover marked on a LIDAR-DEM image, based on IT System of the Country's Protection against Extreme Hazards data. B – Simplified tectonic map of the Mnin stepover. C – Sketch displaying formation of the map-scale folds with helicoidal geometry of the axial surfaces within the restraining stepover. D – Geological map of the Bolmin Syncline area (based on Czarnocki 1961; Różycki 1961, modified). E – Simplified tectonic map of the Bolmin Syncline area

and Chmielnik strike-slip faults (Text-fig. 1). The analyses were based on field observations in quarries and outcrops, where Jurassic rocks (Gruszczyn, Małogoszcz, Głuchowiec, Bocheniec, Karsznice, Starochęciny, Lipowica, Górki), and Jurassic and Miocene rocks (Celiny) are exposed (Text-figs 3, 4, 5). Samples of slickensides for thin section preparation were collected from: i) minor strike-slip fault surfaces with well-preserved kinematic indicators, and ii) strike-slip faults reactivated as normal faults, filled with coarse-grained calcite with rare kinematic indicators on their surfaces. The samples were oriented in relation to the fault strike and dip azimuth for precise geometric and kinematic characteristics of the microstructures. Samples of host rocks for stable isotope analysis were taken from places distant

from the fault surfaces. However, the dense pattern of faults along with their complex damage zones within some exposures limited the sampling distance.

Microstructural analysis

Thin sections were cut parallel to slickenlines and perpendicular to the sampled fault surfaces. Microstructural analysis was performed using a total of 70 thin sections. Structures within the fault zones were viewed using a NIKON ECLIPSE LV100 POL Optical Microscope with a scanning table. Acquisition of images was performed by NIS Elements software. Large images allowed for a detailed geometrical and kinematic analysis of the fault zones and of the textural characteristics of the calcite infilling the faults and fractures. The assembled microstructural data along with field data were the basis for further selection of calcite samples for fluid inclusion analyses. The microstructural dataset provided in this study is representative for fault zones dissecting the Permo-Mesozoic cover in the south-western part of the HCFB.

The results of microstructural observations based on transversal cross-sections of the cores and damage zones of selected minor faults are presented separately for strike-slip and normal faults. The microstructures were described in relation to damage location: i) along fault surfaces and related to oversteps of their segments; and ii) subsidiary faults and shear fractures (Riedel 1929; Bartlett *et al.* 1981) that developed within host rocks in close vicinity to the fault surfaces. Small-scale shear fractures, as ubiquitous and unequivocal kinematic indicators (Petit 1987; Passchier and Trouw 1996; Doblas *et al.* 1997), were the main tool used to verify the sense of displacement along faults established during fieldwork. Shear fracture-related calcite veins and their textures aided in the kinematic interpretation of the fault zones.

Fluid inclusions analysis

Phase transitions in fluid inclusions were measured in doubly polished wafers using a LINKAM THMSG-600 freezing/heating stage mounted on an Olympus BX-51IR microscope. The stage was calibrated against pure chemical compounds with known melting temperatures and natural fluid inclusions with known compositions. Measured temperatures were within 0.1ºC of the 0ºC (distilled water) and -56.6ºC (inclusions of pure carbon dioxide) standards. The estimated accuracy of measurements on unknowns was within ±0.1ºC during freezing runs and ±0.5ºC during heating runs.

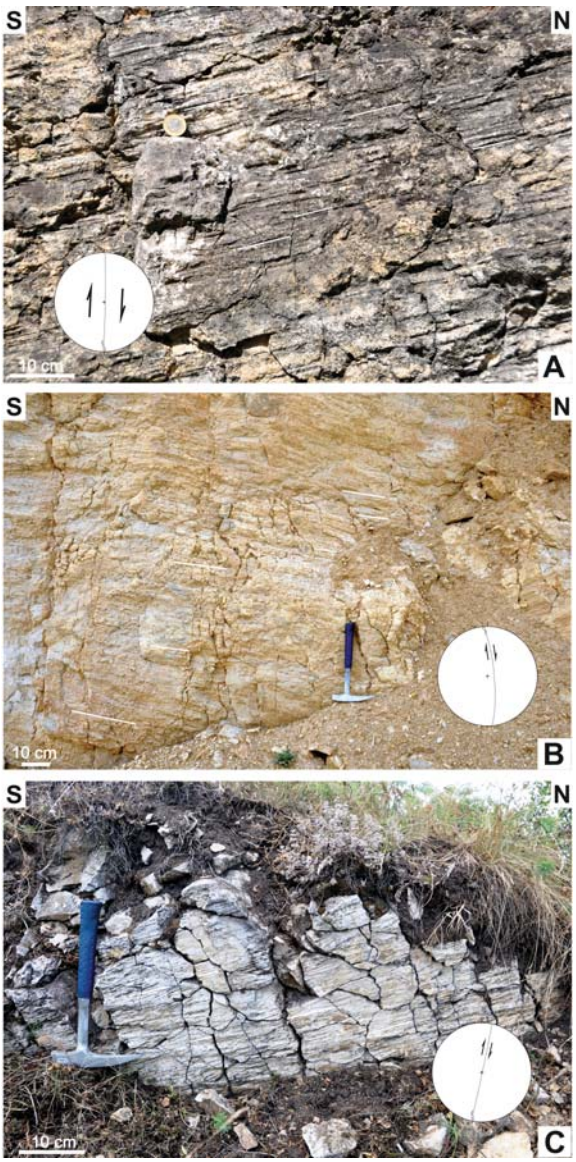

Text-fig. 3. Examples of slickensides of dextral strike-slip faults dissecting Jurassic limestones. A – Slickenside of a second-order dextral strike-slip fault R in Sobków Quarry. B – Slickenside of a second-order dextral strike-slip fault R in Głuchowiec Quarry. C – Slickenside of a second-order dextral strike-slip fault R in Karsznice. For location see Text-fig. 1A

UV-induced fluorescence was investigated on thick sections using an Olympus BX-51IR polarisation microscope equipped with a set of long-working-distance UV- and IR-transparent lenses. An ultra-high vacuum mercury lamp produced wide-band radiation, from which the UV-radiation with a wavelength of 365 nm was extracted using a

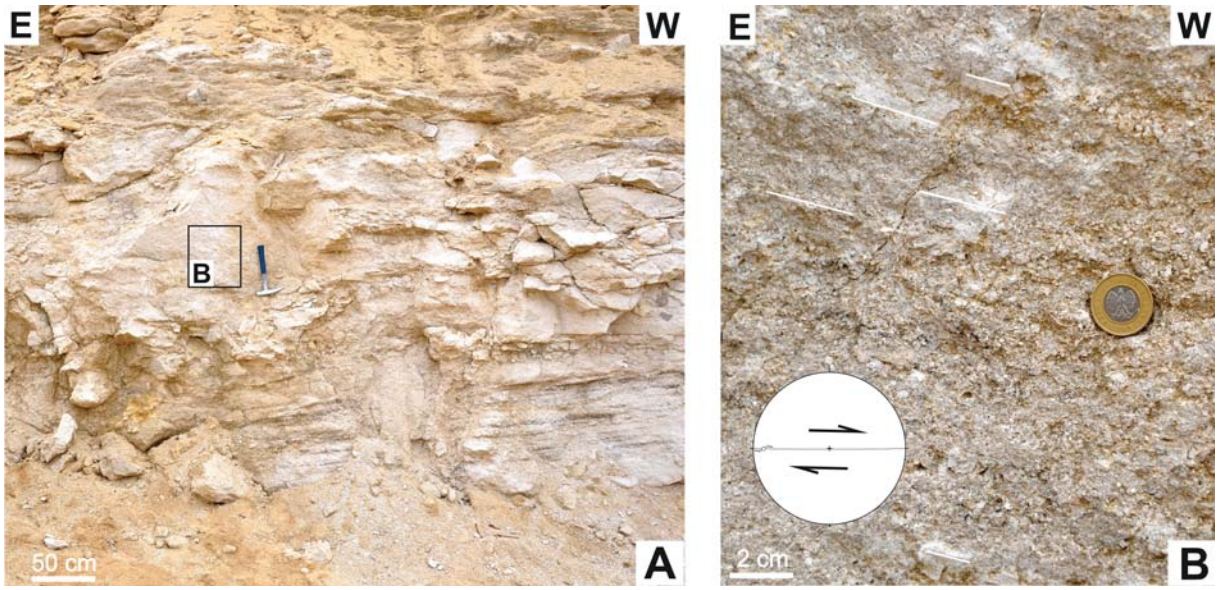

Text-fig. 4. Example of strike-slip faulting in the Celiny Quarry. A – Miocene rocks. B – Slickenside of the main dextral strike-slip fault dissecting the Miocene rocks

U-MWU2 mirror unit with a DM400 dichroic mirror, BP330–385 nm excitation filter and a barrier filter to block out the electromagnetic radiation over 420 nm wavelength.

Raman spectra were recorded in thick sections using a Horiba Jobin-Yvon Xplora spectrometer equipped with an Olympus BX-51 Optical Microscope. Samples were illuminated with a 18 mW diode-pumped solid-state Nd-YAG laser with fundamental emission at 1064 nm, frequency-doubled to 532 nm. A long-working-distance LMPLanFI 100 × 0.8 objective was used to focus the laser beam and to collect the scattered light with a Peltier-cooled (-70ºC), multichannel CCD detector (1024 × 256 pixels) at spectral resolutions between 3 and 1.2 cm^{-1} (600 and 1200 gr/mm gratings). The spectrometer was calibrated periodically using the principal line of silica at 520.7 cm^{-1}.

Stable isotope (δ18O and δ13C) analysis

The source of the fluids and dissolved inorganic carbon (DIC) that provided substrates for calcite precipitating within fault zones was investigated by stable carbon and oxygen isotope analysis performed in the GeoZentrum Nordbayern, University of Erlangen-Nürnberg, Germany. Carbonate powders were reacted with 103% phosphoric acid at 70ºC using a Gasbench II connected to a ThermoFinnigan Five Plus mass spectrometer. All values are reported in per mil relative to V-PDB by assigning a $\delta^{13}C$ and $\delta^{18}O$ values +1.95‰ and -2.20‰ to NBS19 and -46.6‰ and -26.7‰ to LSVEC standards, respectively. Reproducibility and accuracy monitored by replicate analysis of laboratory standards calibrated to NBS19 and LSVEC is better than ± 0.07‰ for $\delta^{13}C$ and 0.05‰ for $\delta^{18}O$ (1σ).

RESULTS

The applied methods gave qualitative and quantitative data that allowed for characterising the source and pathways of fluids precipitating calcite in relation to the structural patterns of strike-slip and normal faults; further discussion was based on these data.

Structural data

The strike-slip faults dissecting the Permo-Mesozoic rocks in the south-western part of the HCFB form a complex anastomosing fault pattern consisting of non-planar faults and segmented strike-slip fault systems (Konon and Mastella 2001; Mastella and Konon 2002; Konon 2015; Konon *et al.* 2016). The fault pattern comprises N-S, NW-SE and WNW-ESE-striking faults west and north-west of the HCFB and near WNW-ESE-striking faults south-west of the fold belt (Text-fig. 1). Slickensides of major strike-

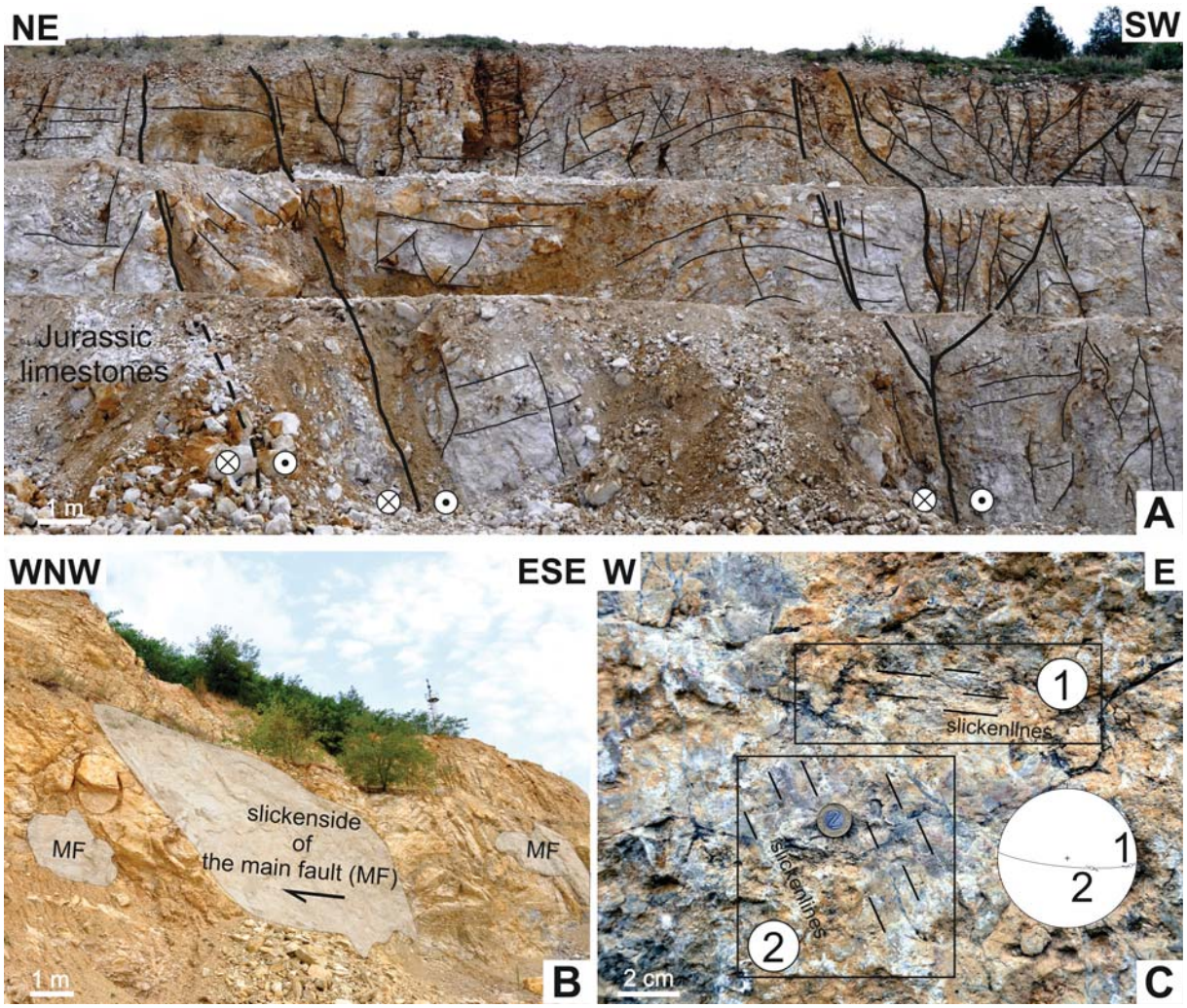

Text-fig. 5. Details of the Chmielnik Fault Zone revealed in Celiny Quarry. A – Negative flower structure included in the major strike-slip Chmielnik Fault zone. B – Slickenside of the main dextral strike-slip fault dissecting Jurassic rocks. C – Example of slickenside of subsidiary fault with a strike-slip component (1 – older) and normal-sense component (2 – younger)

slip faults are more weakly preserved in comparison to the slickensides of the second-order faults formed within the main damage fault zones (Text-figs 3, 5B, C). The sense of movement indicates that the near N-S subsidiary striking faults are dextral strike-slip faults corresponding to Riedel shears (Riedel 1929). The relation of part of them with the strikes of major faults suggest that these second-order minor faults formed also as Riedel-type shears in a transpressional regime (Text-fig. 5B, C).

The non-planar geometry of most of the major fault planes facilitated the formation of releasing or restraining bends, well-recognised, for instance, along the Gnieździska-Brzeziny Fault (Mastella and Konon 2002; Konon *et al.* 2016; Rybak-Ostrowska *et al.* 2017). Fault segmentation favoured the development of stepovers such as the Mnin restraining stepover (Konon *et al.* 2013, 2014; Konon 2015; Konon *et al.* 2016) and the Chmielnik releasing stepover described for the first time in this paper (Text-fig. 5).

The Chmielnik stepover was recognised based on observations in the Celiny Quarry and on cartographic data (Romanek 1982). The elongated WNW-ESE-trending graben is within the hinge of the Piotrkowice Syncline (Romanek 1982). In the central part of the graben, Upper Jurassic rocks form the hanging wall relative to the footwall blocks built of Triassic rocks (Text-fig. 6). We interpret this exten-

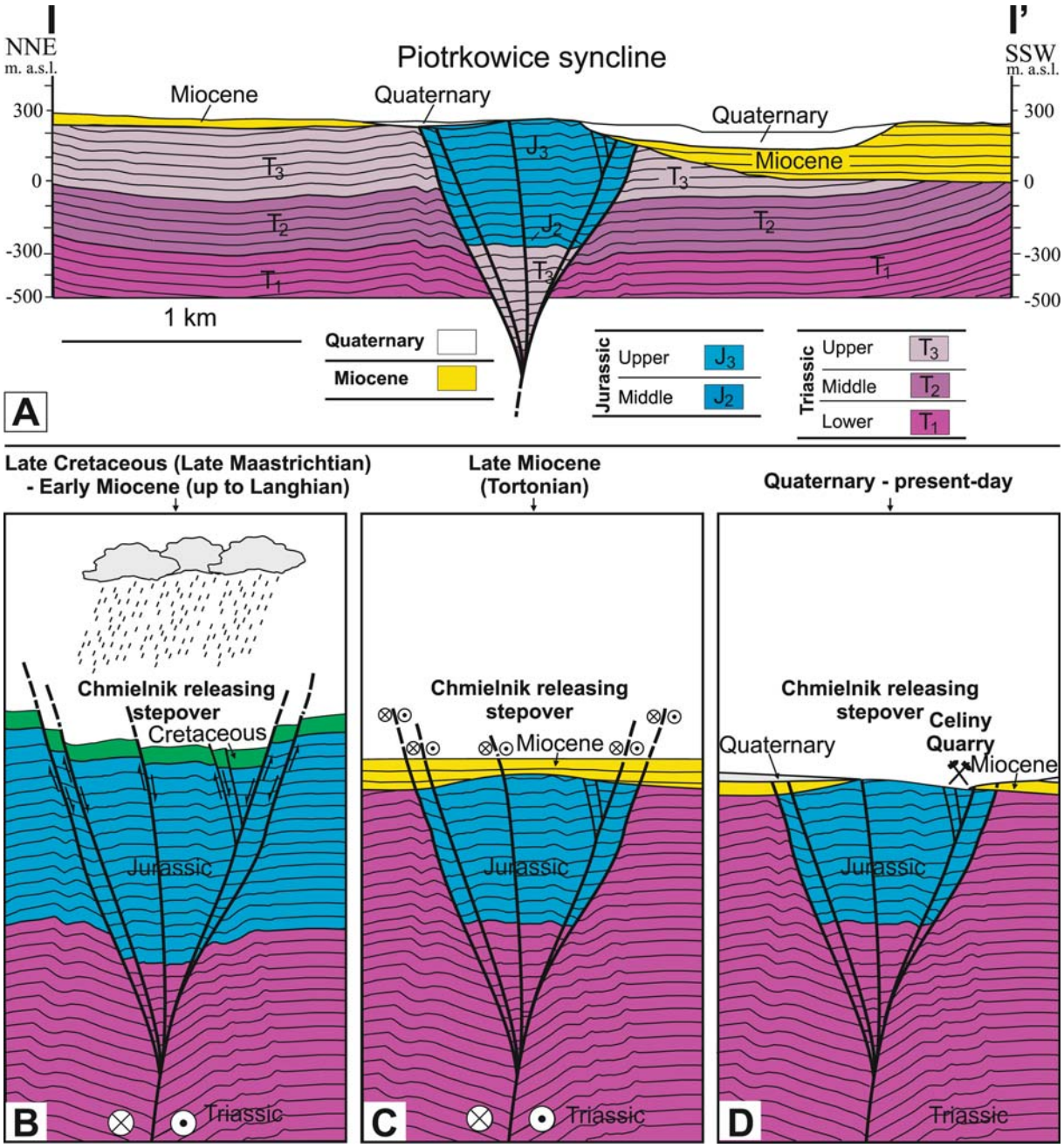

Text-fig. 6. Chmielnik releasing stepover. A – Simplified geological cross-section based on Romanek (1982), modified. B-D – Proposed model of the development of the Chmielnik releasing stepover

sional structure as a releasing stepover between the northern and southern segments of the dextral strike-slip faults included within the Chmielnik strike-slip fault zone (Text-fig. 1).

The dissection of folds developed in the Permo-Mesozoic cover of the HCFB by major strike-slip faults suggests that the strike-slip faulting occurred after the folding (Text-figs 5A, 6A).

The situation in Celiny Quarry is unique; here it is possible to observe the southern part of the releasing stepover where the subsided area is bounded by two parallel strike-slip faults belonging to the Chmielnik

strike-slip fault system. The faults recognised in the quarry dissect both Jurassic and Miocene rocks (Text-figs 4B, 5A–C). Folded Jurassic rocks represent Lower Kimmeridgian strata with a thickness reaching up to several hundred metres, which are overlain by shallowly S-dipping middle Miocene (Serravalian) rocks (Text-fig. 6) (e.g., Senkowicz 1955).

The step length and width correspond to ~7 km and ~1 km, respectively. Individual strike-slip faults included in the major strike-slip fault zones form negative flower structures (Text-fig. 5A). The strike-slip faults also have a normal sense component, in some places younger than the strike-slip component (Text-fig. 5B, C).

Major map-scale strike-slip faults show wide, up to several tens of meters, fault zones with cores defined by fault rocks and damage zones comprising a complex pattern of subsidiary shear fractures (Mastella and Konon 2002; Konon *et al.* 2016). Second order map-scale strike-slip faults show a dominantly simple architecture defined by the main surface and subsidiary shear fractures mineralised with calcite within the damage zone. Calcite mineralisation is abundant along the main fault surfaces and diminishes with increasing distance from the cores (Konon *et al.* 2016; Rybak-Ostrowska *et al.* 2017). Some of the exposed strike-slip faults show the presence of gouges (Text-fig. 5A), however such faults are beyond the scope of this study.

Characteristics of damage zones

The strike-slip faults dissect carbonate rocks of Oxfordian (Miedzianka, Starochęciny, Lipowica), Kimmeridgian (Głuchowiec, Celiny, Karsznice, Sobków) and Miocene age (Celiny) (Text-fig. 1).

Exposures of fault zones display shallow-generated damage zones with widths up to several tens of metres, cutting Oxfordian mudstones and grainstones with cherts and Kimmeridgian oolitic grainstones (according to the classification of Dunham 1962). The exposures show individual continuous or segmented slip surfaces defined by predominantly well-developed slickensides with slickenfibres, preserved slickenlines and steps resulting from the intersection of Riedel shears (Text-figs 3A–C, 5C). Additionally, some of the fault surfaces bear traces of pressure solution (Text-fig. 3C). Fault cores and subsidiary structures within the fault zones mineralised with calcite have been the main object of sampling and the basis for further microstructural analysis. Commonly, the calcite is rather coarse grained, blocky to elongated, white in colour within all exposures of the strike-slip fault zones. The only exception is calcite within the cores of normal faults exposed in Celiny Quarry, which is elongated to fibrous and changes its colour from white to honey-like. Some of these veins are exposed along the central lines of the veins; in this case they show sugar-like surfaces.

Microstructural observations

Thin sections of cores and damage zones reveal their structural pattern and give insight into the internal structure of the veins (Text-figs 7–11) allowing us to follow the evolution of deformation within the fault zones.

Strike-slip faults

The cores of second order strike-slip faults show calcite veins with oblique arrangement of blocky crystals consistent with the sense of fault movement (Text-fig. 7A, B). The size of calcite crystals ranges from tenths of a millimetre to several millimetres. The veins show host rock inclusions incorporated in thin bends between the calcite crystals.

Commonly, minor strike-slip faults and associated subsidiary shear fractures show segmentation and often develop extensional overlaps. The overlapping arrangement of the segments has resulted in the formation of fault-parallel calcite veins (Text-figs 8A, 9A) defined as dilational jogs (e.g., Segall and Polard 1980). This type of vein occurs individually (Text-figs 8A) or in sets (Text-fig. 9A) that form sheets separated by slip surfaces (e.g., Passchier and Trouw 1996; Bons *et al.* 2012). The walls of these veins are defined by fractures inclined at angles of c. 45–50º to the fault surface and occasionally arranged in arrays. As a result, the multilayered vein structure shows a staircase geometry. The fracture traces are wavy in the mudstones and more irregular within the oolitic grainstones as a result of the local bypassing of individual larger grains.

The individual dilational jogs show a rhomboidal geometry infilled with blocky to elongated or less commonly fibrous calcite. The calcite shows a fault-parallel or slightly oblique arrangement within the veins (Text-figs 8A, 9A). The veins show bitaxial or unitaxial growth of calcite. The size of the calcite crystals varies across the veins and shows dependence on the available space. The calcite within dilational jogs contains elongated or sigmoidally shaped host rock inclusions arranged subparallel to the initial fracture surface. The size of the host rock inclusions reaches up to tenths of a millimetre. The arrangement of calcite crystals and the veins association with slip

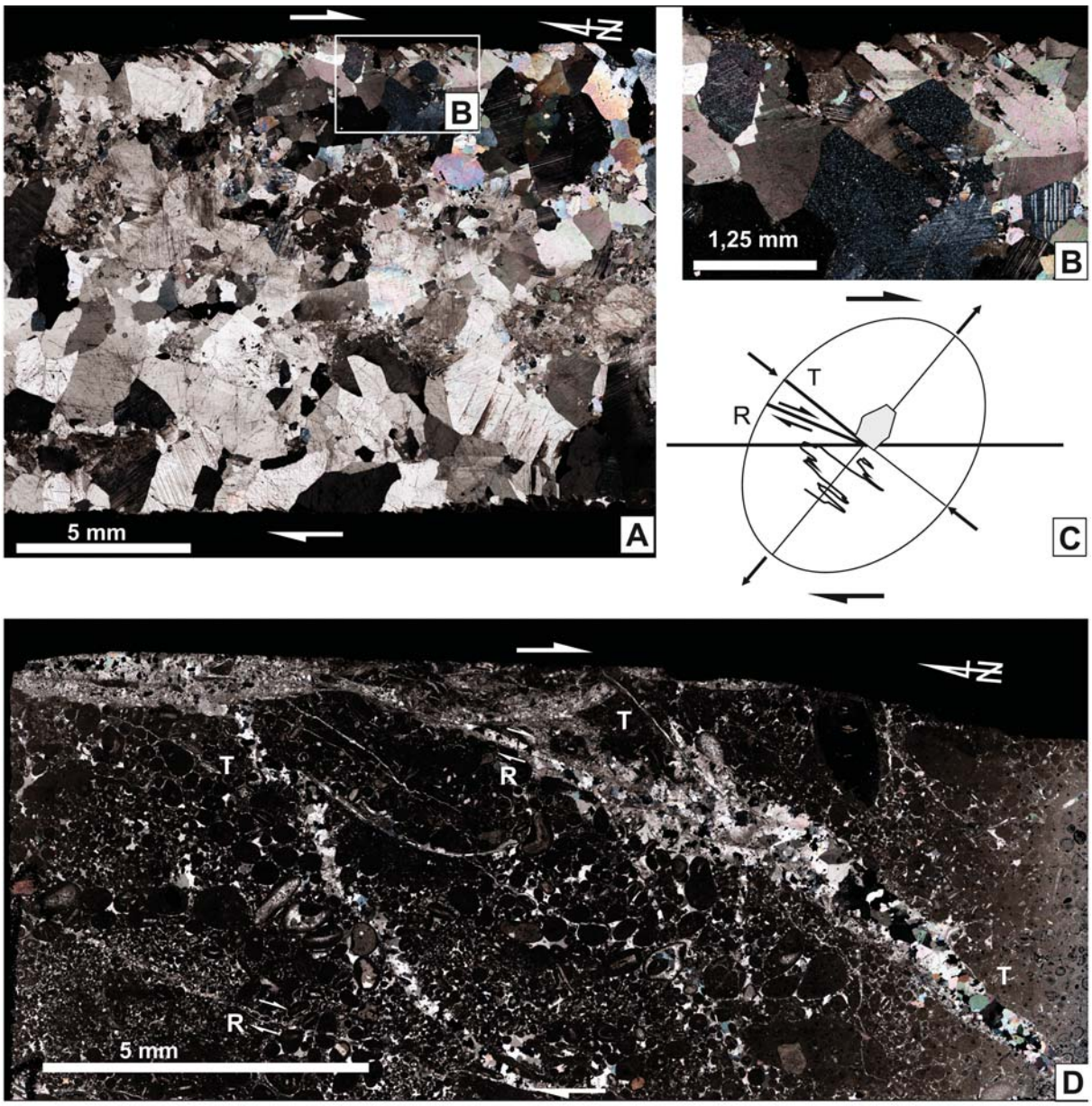

Text-fig. 7. Second order dextral strike-slip fault zone developed within Kimmeridgian oolitic grainstones in Głuchowiec Quarry (sample 33). A – Fault-parallel calcite vein infilled with blocky-to-elongated crystals. B – Stylolite developed along calcite vein. C – Strain ellipsoid based on small scale shear fractures and calcite crystals arrangement within damage zone. D – Structural pattern of damage zone composed of R shear fractures and T fractures

surfaces along with the presence of host rock inclusions indicate syntectonic growth of calcite within dilational veins that have been interpreted as syntaxial (after Durney and Ramsey 1973).

Damage zones contain subsidiary shear fractures classified according to Riedel (1929) and Bartlett (1981). The pattern of shear fractures varies in individual exposures. Nevertheless, carbonate rocks show a broad spectrum of the shear fracture pattern including R, R', X and P shear fractures and T fractures, accompanied by syntectonic calcite growth (Text-figs 7D, 8A, C, 9A–F, 10A–D).

The R shear fractures are inclined at an angle of 20–30º to the main slip surfaces (Text-figs 7–9) and

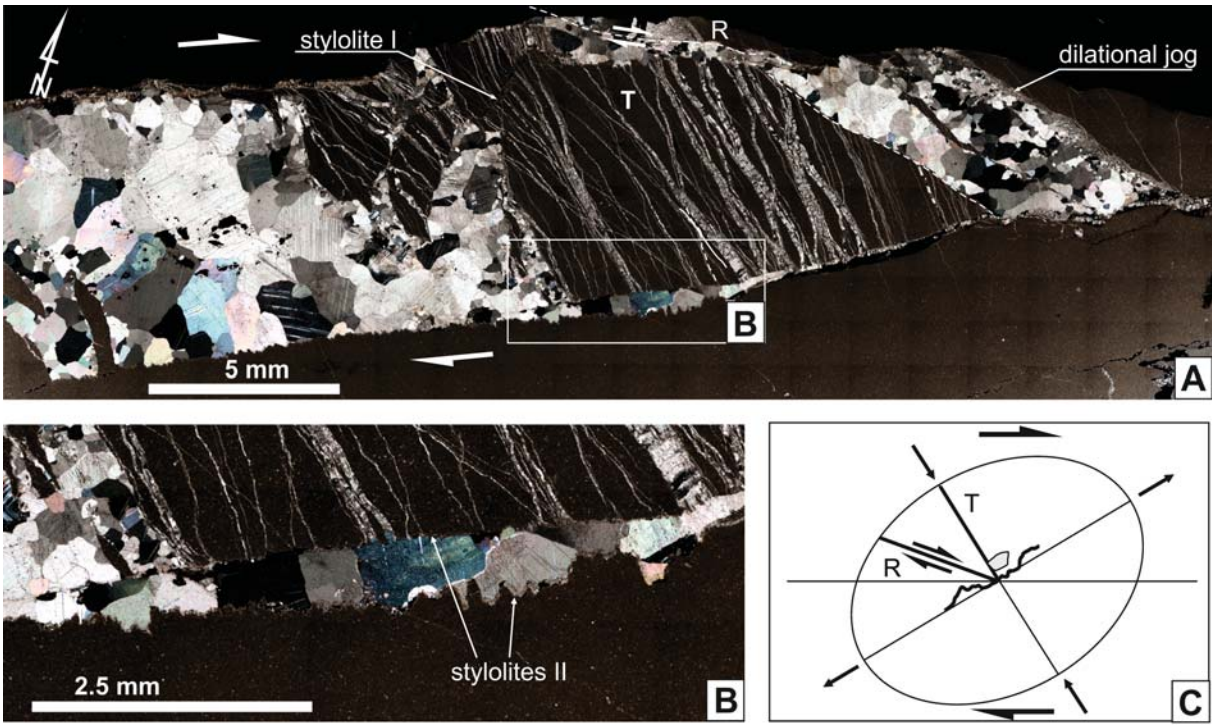

Text-fig. 8. Damage zone of dextral strike-slip fault developed within Oxfordian limestones in Głuchowiec Quarry (sample 42). A – T fracture-mesh and related dilational jogs infilled with blocky calcite. Stylolites are perpendicular to T fractures within the mesh. B – Details of fault-parallel stylolites and their relation to T fractures. C – Strain ellipsoid based on small scale structures within damage zone

occur in regular sets. They show continuous traces or an *en* éch*elon* arrangement resulting in the formation of dilational veins within overlaps of the segments. R shear fractures are infilled with: i) blocky calcite that locally shows bitaxial growth; or ii) elongated calcite that shows unitaxial growth between the fracture walls (Text-figs 8A, B, 9A, C, E). The veins are syntaxial.

The R' shear fractures occur in regular sets: i) between segments of R shears (Text-fig. 9), ii) in association with R shears and T fractures (Text-fig. 10D) resulting in the formation of a complex pattern similar to that described as fault and fracture meshes (Sibson 1996, 2000). Individual sets of R' shear fractures commonly make a high angle with the sampled fault surface; however some examples of low angle fractures have also been noted. Dominantly R' shear fractures are inclined at 70–85º to the fault surface. Commonly, the traces of R and R' shear fractures are irregular and show a tendency for mutual coalescence or changes of dip at points of fracture contacts within a system with the domination of R' shear fractures (Text-figs 10A, B, D). As a result, a braid-like fracture mesh is formed. The effect is multiplied within the oolitic grainstones by fractures bypassing larger grains and decreasing apertures of fractures that cut the grains. Both cases result in more wavy traces of the fractures (Text-fig. 10B).

R' shear fractures with tenths of a millimetre-wide apertures are infilled predominantly with blocky calcite, whereas fractures with millimetre-wide apertures are infilled with elongated and fibrous calcite. Blocky calcite shows irregular shapes and a tendency for sub-perpendicular or slightly oblique arrangement to the fracture walls. Elongated and fibrous calcite shows a sub-perpendicular arrangement to the fracture walls. Locally, blocky, elongated or fibrous calcite coexist within individual fractures.

T fractures are common within damage zones (Text-figs 7D, 8A, 9A, B, D, 10A, B, D, E, F). They show variable inclinations, from 40 to 60º, to the fault surface. Traces of T fractures are irregular, with the most variable within oolitic grainstones. The apertures of the fractures vary within samples from tenths of a millimetre to a few millimetres. The fractures are infilled with blocky to elongated calcite. The calcite shows subperprendicular arrangement to the fracture walls. Elongated fragments of wall rocks are incorporated within the veins.

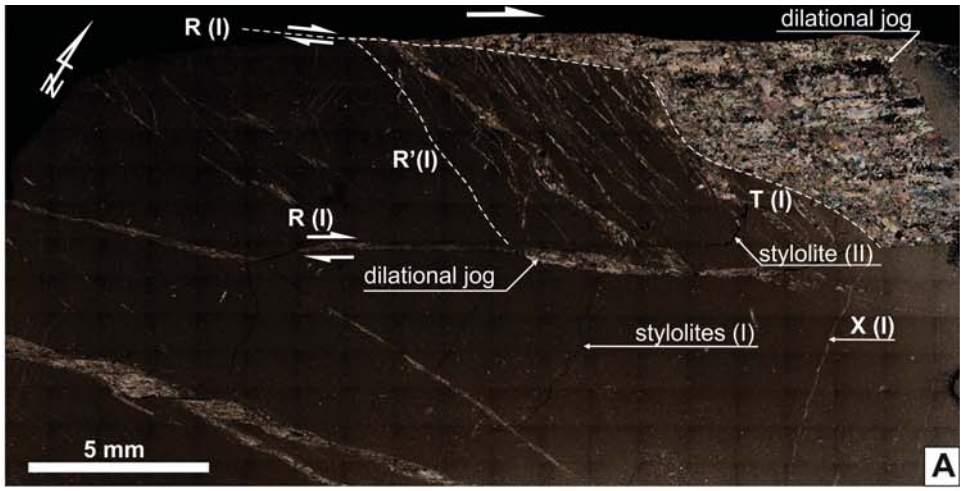
R (I)
dilational jog
R'(I)
T (I)
R (I)
stylolite (II)
dilational jog
stylolites (I)
X (I)
5 mm
A

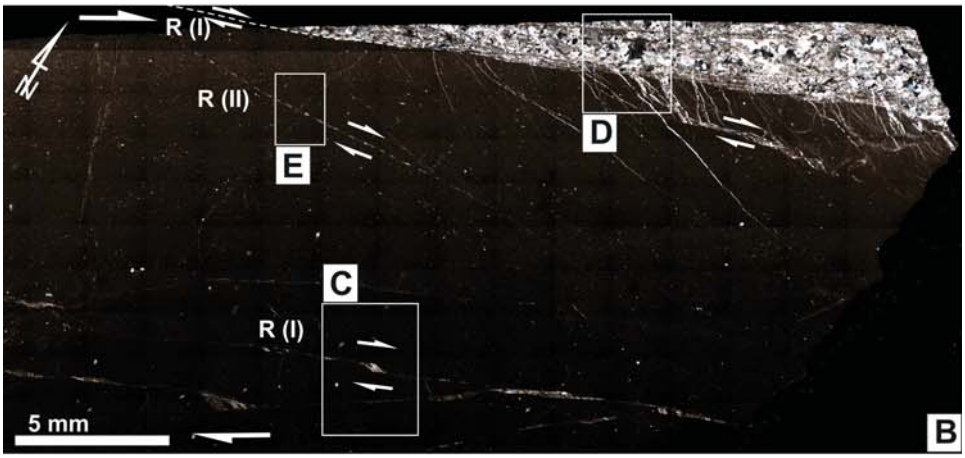
R (I)
R (II)
E
D
C
R (I)
5 mm
B

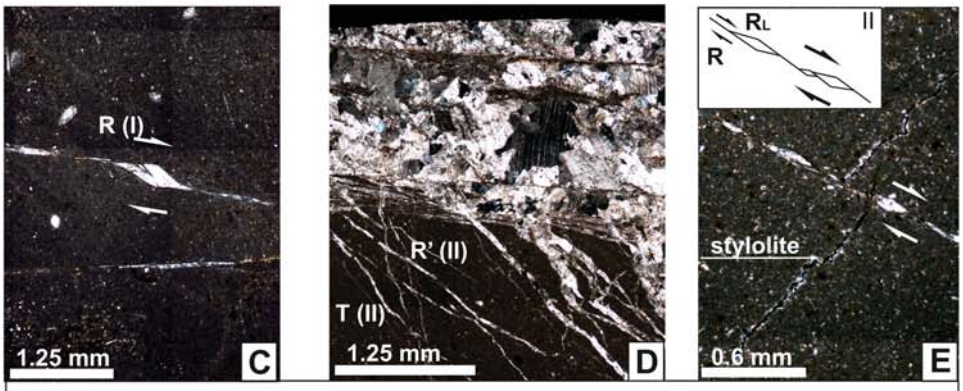
R (I)
1.25 mm
C
R' (II)
T (II)
1.25 mm
D
R
II
stylolite
0.6 mm
E

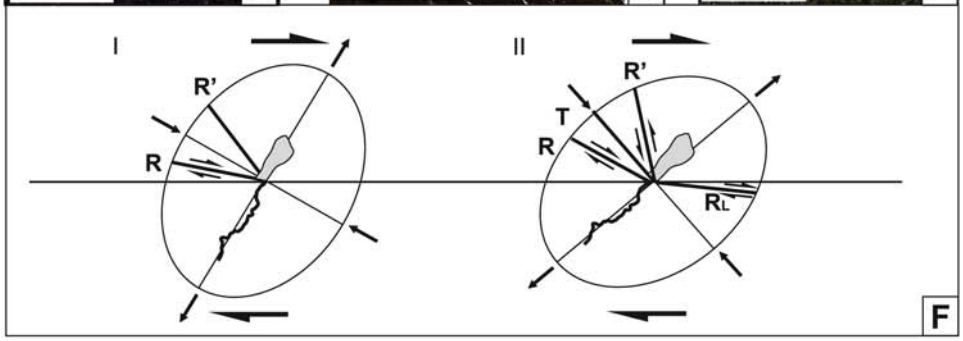
I
R'
R
II
R'
T
R
F

X shear fractures occur occasionally (Text-fig. 9A). They are inclined at 80–85º to the fault surface and dip in the opposite direction in relation to the sampled fault. The traces of the X shear fractures are irregular and their apertures do not exceed 0.1 mm. X shear fractures are infilled with blocky calcite forming syntaxial veins. These shear fractures crosscut previously formed R and R' shear fractures, and T fractures.

P shear fractures occur in sets inclined at 25–30º to the slip surface, which results in a secondary feature that is superimposed on the previously developed R and R' shear fractures, and T fractures (Text-fig. 10A–C). P shear fractures are blurred and show variable outlines. Some of them are widely extended and form a kind of a structural veil (Text-fig. 10A–C). The calcite infilling of P shear fractures is dominantly blocky, although elongated grains have also been noted.

Calcite within fault parallel veins and subsidiary shear fractures shows deformation lamellae that are predominantly straight and only locally wedge-shaped (Text-figs 7A, B, 8A, B, 10E, F). Secondary assemblages of fine grained mosaic-like calcite occur locally (Text-fig. 7A, 9A, 10E, F). Both deformation lamellae and assemblages of mosaic calcite indicate deformation within fault zones postdating the calcite precipitation.

Veins and host rocks within fault zones commonly display evidence for localised stress-induced dissolution (Text-figs 7A, B, 8A, B, 9A, E, 10A, B). Stylolites occur perpendicular to T fractures within the damage zones. However, there are some examples of stylolites that developed along pre-existing faults and subsidiary shear fractures and related veins (Text-figs 7A, B, 8A, B). Commonly, they occur along boundaries of veins and host rocks, or within the veins. They indicate slow deformation (e.g., Koehn *et al.* 2007; Ebner *et al.* 2010) of rocks and veins within fault zones and related local mass transfer acting during the fault activity.

The strain ellipsoids related to strike-slip faults show a general trend of formation of the subsidiary small-scale structures predominantly within the shortening quadrant of instantaneous strain (Text-figs 7C, 8D, 9F, 10F). However, the presence of subsidiary shear fractures within extension quadrants of instantaneous strain have been also recorded (Text-fig. 10F). All structures are infilled with calcite that grew almost parallel or slightly oblique to the long axis of the strain ellipsoid.

Normal faults

Normal fault-related calcite veins show apertures up to 4 cm wide. Thin sections of the veins display variable calcite arrangements related to: i) formation of the dilational jogs related to the subsidiary shear fracture pattern (Text-fig. 11A), and ii) development of mode I veins that terminated the faulting stage (Text-fig. 11A, C–F).

Veins associated with shear fractures occur individually or as complex sets of fault-parallel sheets. They often represent complex dilational jogs. The calcite shows a sub-perpendicular arrangement in relation to the vein walls. Calcite crystals reach up to tenths of a millimetre in size, and are blocky or elongated. They show bitaxial or unitaxial growth. The arrangement and shape of the crystals allows the interpretion of the veins as syntaxial.

The mode I veins occur individually or in parallel sets. These veins reveal distinct coarse crystalline calcite. The primary calcite is blocky to elongated, growing sub-perpendicularly to the vein walls towards the centre of the veins (Text-fig. 11C–F). The calcite crystals reach up to a few millimetres in size. Rare euhedral calcite points to a syntaxial growth. Some of the veins show mutual overgrowth of calcite crystals that affects the vein fabric (Text-fig. 11C, E, F). The arrangement of primary calcite within veins reflects a mode I opening and indicates that their opening rates were compensated by the simultaneous calcite growth. Moreover it indicates growth competition that points to a long process of vein formation.

Some veins (Text-fig. 11B, G, H) reveal banded calcite similar to that observed within vadose speleothems and rafts (e.g., Gradziński *et al.* 2012), tufas (e.g., Gruszczyński and Mastella 1986; Mastella and Rybak-Ostrowska 2012) or travertines (Hancock 1999; Uysal *et al.* 2007; Gratier *et al.* 2009). The bands reflect the different textures of these veins. Blocky-to-elongated calcite bands occasionally show zones of crystal face truncation that can be interpreted as precipitation hiatuses (Text-fig. 11G, H) (cf. Nuriel

← Text-fig. 9. Details of damage zone of a dextral strike-slip fault developed within Oxfordian limestones in Głuchowiec Quarry (A – sample 39, B-E – sample 35). A – Dilational jogs infilled with primary elongated and secondary mosaic calcite related to R shear fracture. R' shear fractures and T fractures developed within overlap of R shear fractures. Stylolites follow the orientation of X shear fractures within the host limestone and are perpendicular to T fractures. B – Shear fracture pattern and related veins within damage zone. Multilayered vein related to R shear fracture, infilled with irregular blocky-to-elongated calcite. C – Dilational jog associated with R shear fractures. D – steep position of T fractures and R' shear fractures indicating local stress rotation. E – R and R_L shear fracture pattern indicating local stress rotation (based on Shreurs 2003). Stylolite and related calcite vein cutting R and R_L shears. F – Strain ellipsoids based on shear fracture pattern within damage zone

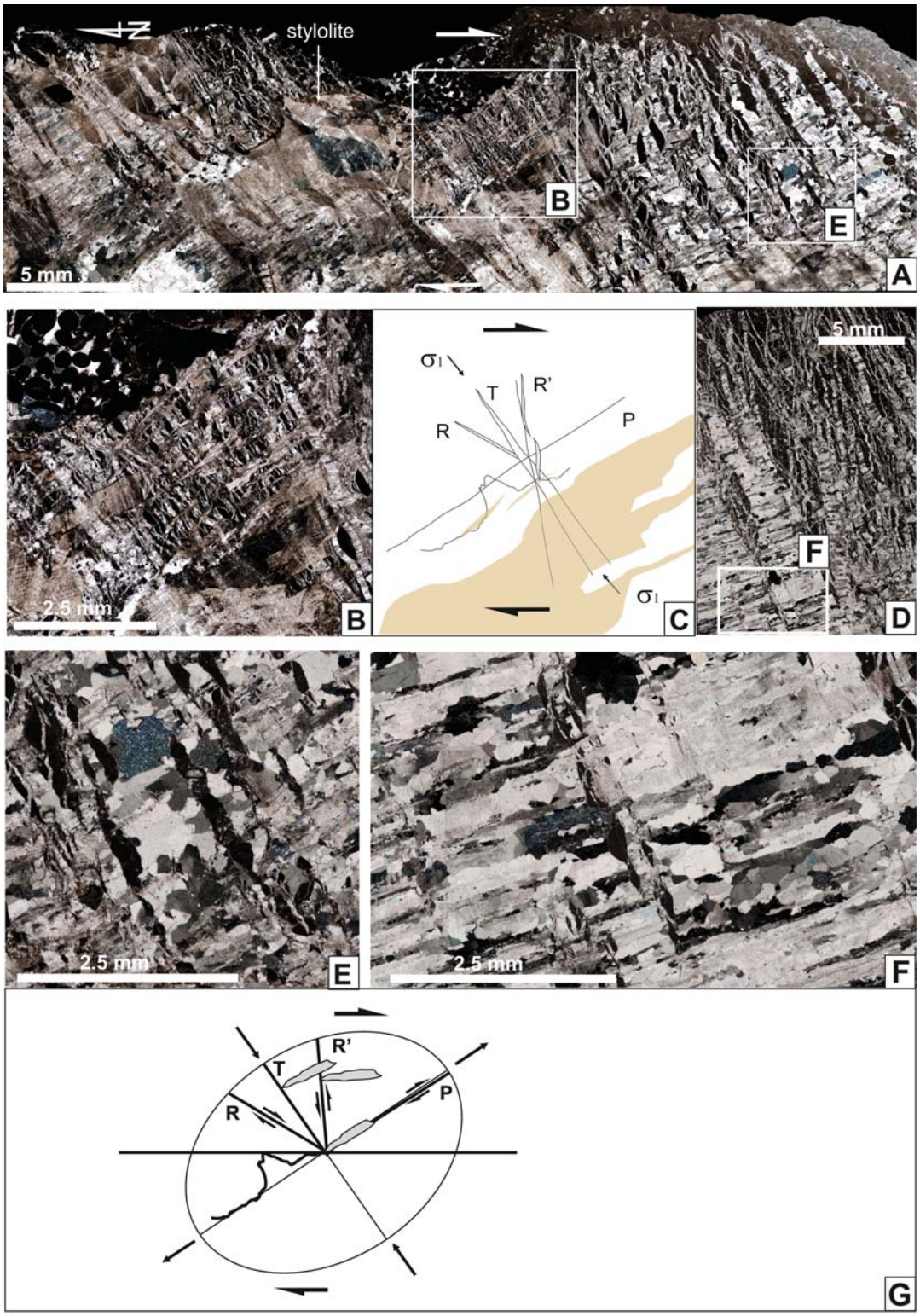

Text-fig. 10. Examples of the shear fracture pattern within the damage zone of a minor dextral strike-slip fault developed within Kimmeridgian oolitic limestones in Sobków Quarry (samples: 18 – A, B, E; 14 – D, F). A-F – Fracture mesh pattern built by R, R', P shear fractures and T fractures infilled with calcite. B – P shear fractures postdating R and R'shear fracture mesh development. Stylolites show perpendicular relation to T fractures. E, F – Examples of calcite infillings: blocky and elongated calcite, respectively, with incorporated host rock inclusions. G – Strain ellipsoid based on shear fracture pattern within damage zone

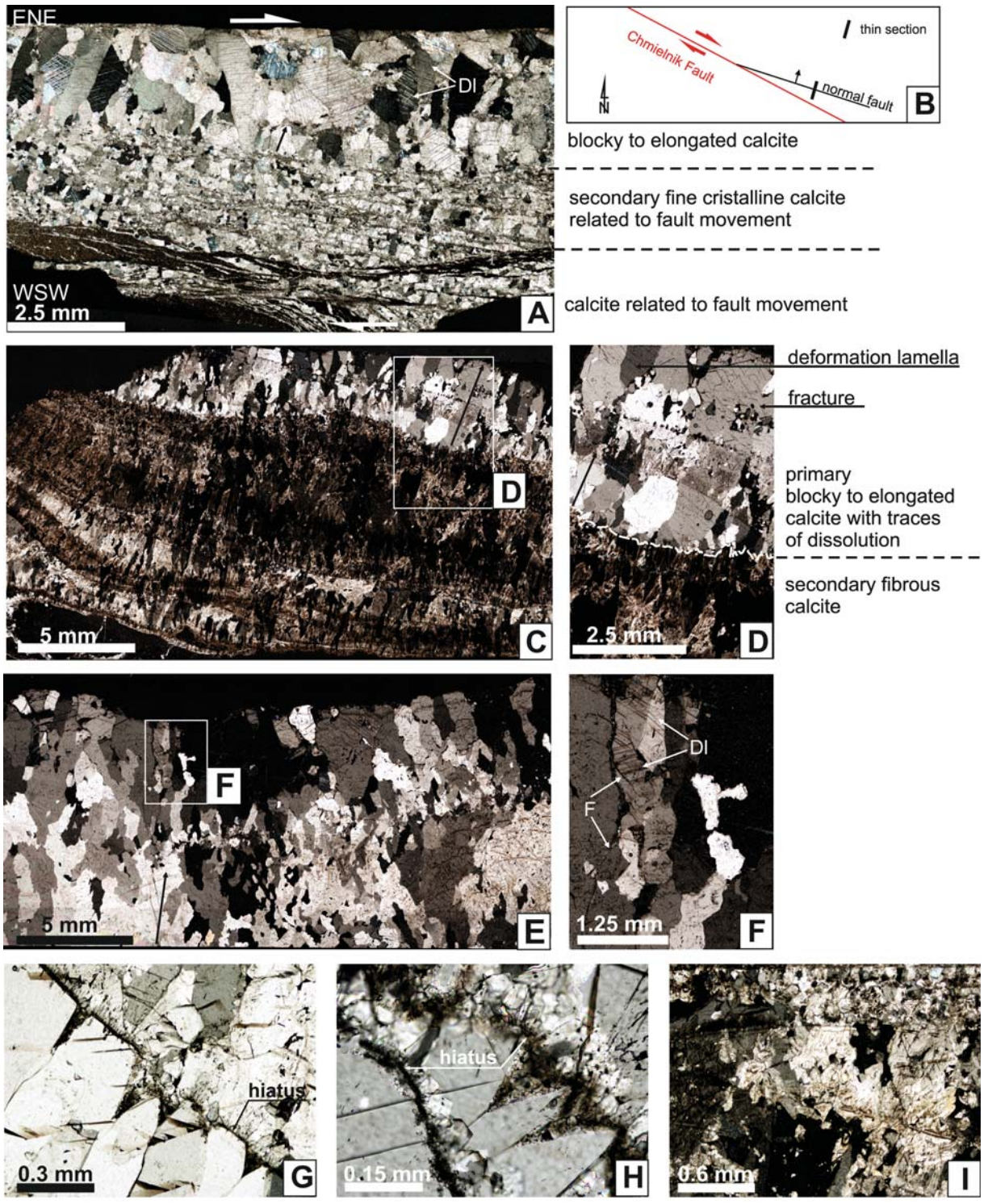

Text-fig. 11. Examples of veins associated with normal faults within Oxfordian limestones in Celiny Quarry (samples: 70 – A, B; 65 – C, D; 66 – E, F; 124 – G, H, I). A – Complex fabric of calcite vein related to fault activity. B – location of thin sections in relation to normal fault orientation. C, D – Syntaxial vein infilled with primary elongated calcite (upper part) covered by secondary calcite (central and lower part). E, F – Syntaxial vein infilled with elongated calcite showing mutual overgrowths. G – Precipitation hiatus within elongated vein calcite with truncated faces. H – Secondary rhombohedral calcite covering primary elongated calcite along precipitation hiatus. I – Transition from elongated into rhombohedral calcite towards the centre of the vein. Arrows on calcite crystals point to their growth direction; abbreviations: F – fractures, Dl – deformation lamella

et al. 2012). The hiatuses show wavy traces and are only locally parallel to the vein walls. The hiatuses as well as the spaces between crystals adjacent to the hiatuses are places for the growth of fine crystalline calcite with a rhombohedral habit (Text-fig. 11H) that locally covers the previously formed blocky-to-elongated calcite. These observations led us to conclude that the hiatuses may record discontinuities in calcite precipitation within the veins that could have been associated with dissolution episodes. Additionally, the blocky-to-elongated textures locally show subsequent replacement and transition into rhombohedral ones towards the centre of the vein (Text-fig. 11I). Moreover, secondary fibrous calcite occurs within zones of altered primary textures (Text-fig. 11D).

The veins related to normal faults, including banded calcite veins, show evidence of deformation within the fault zones after calcite precipitation. Fracturing of calcite crystals occurs in the outer parts of individual veins, commonly at the boundary of the vein and the host rock (Text-fig. 11D, F). Twinning is common: deformation lamellae occur in the outer parts of individual veins (Text-fig. 11D, F) or inside the vein (Text-fig. 11A, D).

These observations allowed us to assume that during the terminal stage of the fault activity blocky-to-elongated calcite grew in open spaces that were the pathways for acidic fluids responsible for the dissolution of primary calcite within the veins. We suggest that the precipitation of rhombohedral and fibrous calcite postdates the growth of blocky-to-elongated calcite within the fault zone studied. However, only application of a precise radiometric dating of vein infilling can yield the ages of the calcite growth sequence.

Fluid inclusion petrography and measurements

Fluid inclusions were relatively rare; they were observed in only 7 samples (sample numbers 18, 29, 41, 51, 52, 57, 61, 65 and 66). The dimensions of the fluid inclusions studied varied from several micrometers up to 50 μm (samples 18, 29) (Text-fig. 12A–F).

Fluid inclusions occur predominantly in the transparent and twinned blocky calcite which grades in places into fibrous and sinter-like calcite. Limonitised pyrite was observed in sample 45, otherwise no other minerals have been detected, either under microscope or by Raman spectrometry. However, observations of fluid inclusions were often obscured by the high birefringence of the host mineral and the total reflection of light along the high-density contrast boundary between the host calcite and 3D fluid inclusions.

Several types of fluid inclusions were distinguished based on phase composition at room temperature. All inclusions were aqueous, consisting of variable proportions of liquid and vapour phases. Monophase aqueous inclusions were relatively frequent. Monophase gaseous inclusions occurred dominantly in fibrous calcite, where they were oriented parallel to the fibres.

Raman spectroscopy of the gas phase and the apparently gaseous inclusions in fibrous calcite have not yielded signals indicative of common gases. Hence, the gaseous inclusions are considered as empty, or as being filled only with very low-density gas or air that does not provide any Raman scattering. Similarly, inspection under UV-light has not revealed luminescence diagnostic of liquid hydrocarbons.

Microthermometric experiments have demonstrated that all aqueous inclusions contain a low-salinity aqueous liquid, with ice melting temperatures close to 0ºC. Metastable superheated ice has persisted in monophase fluid inclusions, as well as in some inclusions with small vapour bubbles to temperatures up to 2.5ºC, due to the high internal pressure imposed by expanded ice. These inclusions often decrepitated on freezing, but the stable temperature of melting of ice, always around 0ºC, could have been measured during the second freezing run. Homogenization temperatures of two-phase inclusions have been recorded in the interval from 85 to 210ºC, depending on the volume of vapour bubbles. Due to negligible salinity, eutectic temperatures of the aqueous solution could not be determined.

Stable isotope composition

Stable isotope analyses of calcite and limestone are listed in Table 1. The limestones exhibit a uniform isotope composition with $\delta^{13}C$ from +2.0 to +3.2‰ (average = +2.5‰, SD = 0.4‰, n = 14) and $\delta^{18}O$ values from -5.0 to -2.3‰ (average = -4.0‰, SD = 0.7‰, n = 13) (Table 1, Text-fig. 12). Only one limestone sample (33A) had an $\delta^{18}O$ value of -7.0‰, that was much out of range. The $\delta^{13}C$ values of calcites were very similar to those of the host limestones, ranging from +2.2 to +3.1‰ (average = +2.6‰, SD = 0.2‰, n = 21). However, the $\delta^{18}O$ values of the calcites were much lower than those of the limestones, ranging from -10.2 to -4.9‰ (average = -7.4‰, SD = 1.0‰, n = 25). Three calcite samples from Celiny Quarry (64, 65, 66) have been exceptional in exhibiting strongly depleted $\delta^{13}C$ values between -8.9 and -8.6‰ compared to other samples (n = 21).

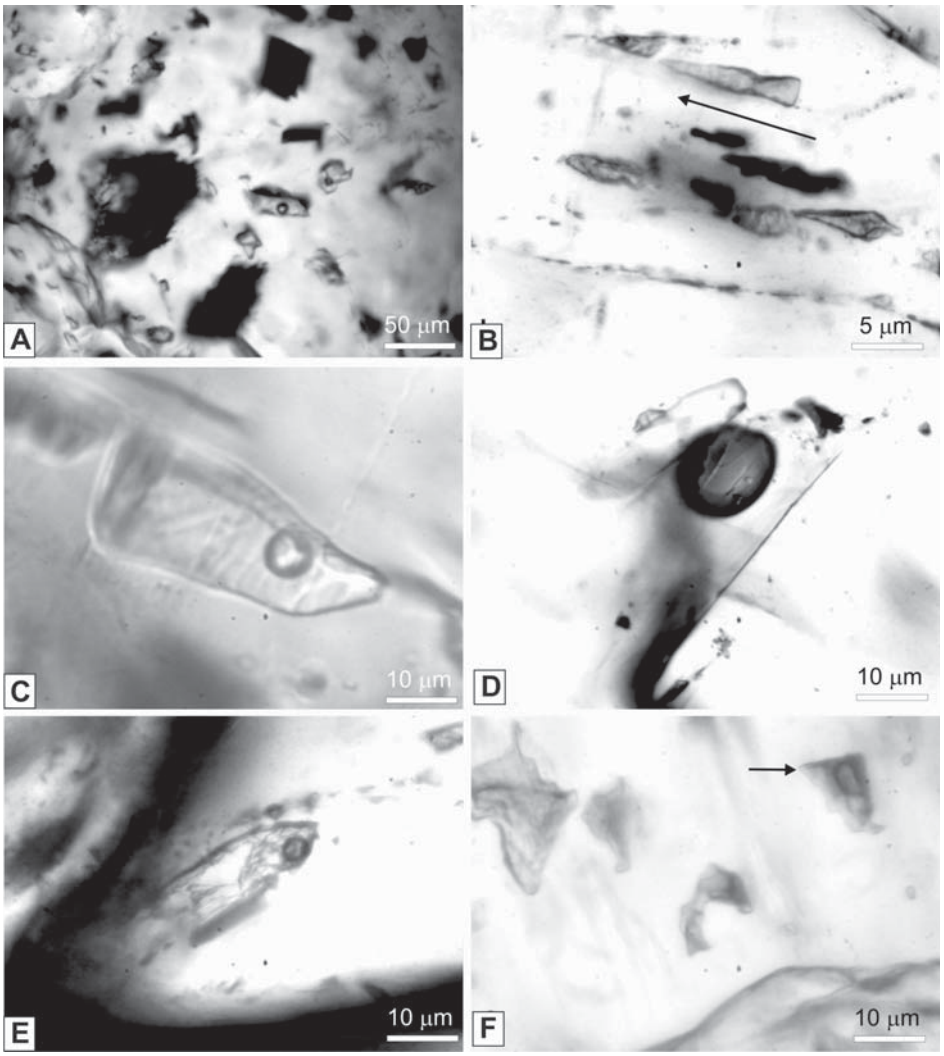

Text-fig. 12. Fluid inclusions. A – Primary two-phase aqueous inclusions in calcite (sample 18). B – Monophase, probably gaseous inclusions, oriented parallel with growth direction (arrow) of calcite fibres (sample 29). C – Large primary, two-phase aqueous inclusion in blocky calcite (sample 29). D – Large two-phase aqueous, probably re-equilibrated fluid inclusion in calcite (sample 51). E – Irregular two-phase aqueous inclusion (sample 52). F – Large monophase aqueous inclusions associated with two-phase inclusions (arrowed) with large bubble indicate crystallization conditions in the vadose zone and simultaneous entrapment of cold groundwater and air bubbles (sample 66)

Whenever a vein-filling calcite was sampled, the neighbouring host rock was also collected. The difference in $\delta^{13}C$ between the limestone and calcite samples is close to zero (from -0.8 to +0.8‰, average = -0.1‰, SD = 0.4, n = 21) with four outliers exceeding the upper limit from +1.5 (Głuchowiec 2-1) up to +11.9‰ (Celiny 8). In contrast, the difference in $\delta^{18}O$ between the limestone and calcite samples is always positive (from +2.0 to +6.2‰, average +3.5‰, SD = 1.1, n = 24), with one outlier exceeding the lower limit at +0.3‰ (Głuchowiec 1-1). In summary, the calcites exhibit almost identical $\delta^{13}C$, but distinctively lower $\delta^{18}O$ values than the corresponding limestones, with a few exceptions (Text-fig. 13).

DISCUSSION

The shallow-generated damage zones of the dextral strike-slip fault zones dissecting the Mesozoic and Miocene rocks in the south-western part of the HCFB provide evidence for fluid pathways related to the fault activity, the origin of fluids and the thermodynamic conditions during the faulting.

Samples		Locality	$\delta^{13}C$ (‰ VPDB)	$\delta^{18}O$ (‰ VPDB)
1	calcite	Starochęciny	2.68	-6.84
1A	limestone	Starochęciny	2.48	-3.93
1B	limestone	Starochęciny	2.51	-4.29
10	calcite	Gruszczyn HCMC	3.10	-7.54
10A	limestone	Gruszczyn HCMC	3.20	-4.32
10B	limestone	Gruszczyn HCMC	3.23	-3.90
11A	limestone	Gruszczyn G15	1.57	-5.37
11B	limestone	Gruszczyn G15	1.87	-4.08
14,1	calcite	Sobków 1	2.62	-7.51
14B	limestone	Sobków 1	2.38	-3.42
18,1	calcite	Sobków 2	2.71	-7.85
31	calcite	Bocheniec	2.30	-6.40
32A	limestone	Głuchowiec 1-1	2.28	-6.97
33	calcite	Głuchowiec 1-1	2.20	-7.27
35A	limestone	Głuchowiec 2-1	2.01	-4.53
36A	limestone	Głuchowiec 2-1	2.35	-4.12
36B	limestone	Głuchowiec 2-1	1.97	-4.54
36C	limestone	Głuchowiec 2-1	2.29	-4.34
38	calcite	Głuchowiec 2	0.80	-7.61
41	calcite	Głuchowiec 1-2	2.90	-7.76
42	calcite	Głuchowiec 3	2.49	-7.55
45,1	calcite	Głuchowiec 1-4	2.46	-7.77
45,2	calcite	Głuchowiec 1-4	2.66	-7.79
52	calcite	Głuchowiec 1-9	2.45	-6.92
53	calcite	Głuchowiec 1-9	2.51	-7.67
54	calcite	Głuchowiec 1-9	2.80	-7.38
55	calcite	Głuchowiec 1-9	2.45	-7.05
55	calcite	Głuchowiec 1-9	2.64	-7.17
55A	limestone	Głuchowiec 1-9	2.49	-4.95
58A	limestone	Karsznice 1	2.70	-4.24
60	calcite	Celiny 3-1	2.34	-8.18
60A	limestone	Celiny 3-1	3.13	-4.07
61	calcite	Celiny 4	2.66	-10.16
61A	limestone	Celiny 4	2.11	-4.61
62	calcite	Celiny 4	2.87	-8.20
64	calcite	Celiny 8	-8.62	-5.70
64A	limestone	Celiny 8	3.05	-2.31
65	calcite	Celiny 8	-8.60	-5.88
66	calcite	Celiny 8	-8.86	-4.87
67	calcite	Celiny 14	2.24	-9.17
68	calcite	Celiny 14	2.34	-7.48
68A	limestone	Celiny 14	2.20	-2.93
69	calcite	Celiny 14	2.28	-7.02
70	calcite	Celiny 14	2.35	-7.22
78A	limestone	Krzyżowa 1	3.15	-3.94
82A	limestone	Krzyżowa 5	3.20	-4.23
92A	limestone	Małogoszcz 3	2.44	-4.78
92B	limestone	Małogoszcz 3	1.94	-4.81
96A	limestone	Małogoszcz 4	2.33	-4.93

Table 1. Oxygen and carbon isotope data

Fluid pathways versus structural pattern within the fault zones

The presence of calcite veins along main faults and subsidiary shear fractures indicates that the fault zones were permeable during fault activity. Faults and related structures cutting Oxfordian mudstones and grainstones with cherts, and Kimmeridgian oolitic grainstones were probably the main pathways for fluids during the deformation.

Calcite infilled the opening fractures, which resulted in the formation of syntectonic veins. The shape and internal structure of the veins indicate that brittle dilatant failure controlled the deformation of carbonate rocks within fault zones (e.g., Pollard and Segal 1987; Scholz 1992). Fractures of the extensional opening mode I, sliding mode II, III and a third, obliquely opening mixed mode were recognised (Text-figs 7, 8, 9, 10, 11). Shear-related veins record repetitive episodes of fracture opening and sealing accompanied by the incorporation of host rock inclusions within the internal structure of the veins indicating a crack-seal mechanism (Ramsay 1980). The later process along with stress-induced solution within the rocks and veins suggests slow subsequent deformation typical of aseismic regimes (cf., Gratier *et al.* 2011; Rybak-Ostrowska *et al.* 2017).

The internal structure of the fault-related calcite veins and their crosscutting relationships (Text-figs 7–11) indicate the formation of veins during subsequent episodes of rock deformation. The sampled strike-slip faults show a sequence of shear fractures: R shears (Text-figs 8A, 9A, B, C, E), R' shears (Text-fig. 11C, D), T fractures (Text-figs 7, 8, 9A, D, 10A, B, D, E, F), and X and P shears that crosscut older shear fractures (Text-figs 9A, 10A, B). Additionally, oversteps of R shears show related subsidiary R' shears (Text-fig. 9) and subsidiary T fractures that crosscut previously formed R' shears. The variable orientation of T fractures with respect to the fault zone indicate local rotation of stress (Text-fig. 7C, 8C, 9F). Moreover, microscopic observations indicate that R shears crosscut previously formed T fractures (Text-fig 8B). This suggests that R shears remained active during fault zone activity (e.g., Ahlgren 2001) and recorded continuous deformation within strike-slip fault zones. Consequently, the increasing strain induced rotation of R and R' shears and T fractures, and enhanced sigmoidal or wavy shapes of the R, R' and T (Text-figs 8A, 9A–E, 10A, D). These observations and interpretations correlate with results of experimental strike-slip fault patterns produced by Schreurs (1994, 2003).

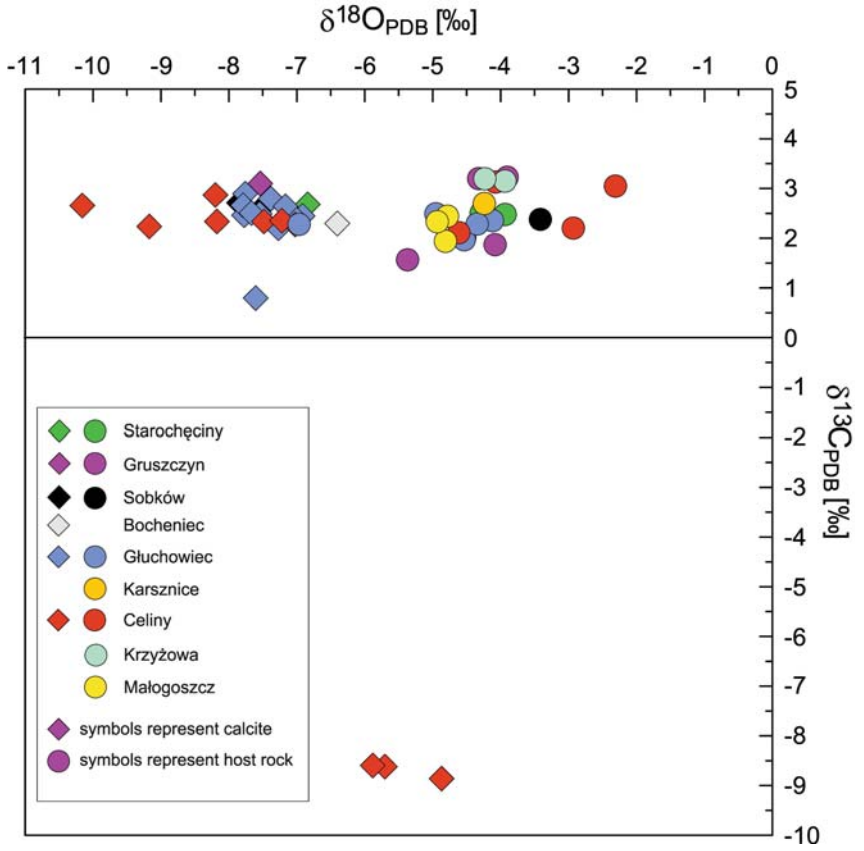

Text-fig. 13. Stable isotope ($\delta^{18}O$ and $\delta^{13}C$ V-PDB) values of calcite veins and host rock limestones

The sequence of shear fractures within fault zones indicates a continuous cyclic process of fault and shear-fracture permeability formation and their sealing by calcite precipitated from fluids within fault zones (cf., Arndt *et al.* 2014). Small scale dilational jogs and subsidiary shear fractures are interconnected locally and might have served as fluid pathways for a limited distance within damage zones. These structures are connected with fault cores that probably provided the main pathways for fluids over the distance governed by fault core apertures and fault extents (cf., Faulkner *et al.* 2010).

The stress-induced solution was cyclically active during faulting (Text-figs 7–10). Based on experimental studies on stylolite-bearing limestones (e.g., Heap *et al.* 2014, 2018), we suggest that stylolites could have acted as additional channels for fluid flow. Stylolites were sites of increased pressure and dissolution, whereas dilational jogs and subsequently formed subsidiary shear fractures were sites of reduced pressure and precipitation of calcite during faults movement at the same time. Thus stylolites along with dilational jogs and subsidiary shear fractures record mass transfer through a fluid phase (cf., Gratier *et al.* 2003, 2013; Crider and Peacock 2004) within strike-slip fault zones in all localities (Text-figs 7–10). This fluid-rock interaction was maintained by horizontal contraction acting during strike-slip faulting.

The trend of continuous transpression (Text-figs 7–10) was related to the progressive inversion of the Polish Basin (Krzywiec 2000, 2002, 2007, 2009; Krzywiec *et al.* 2009; Gutowski and Koyi 2007). Local rotation of stress observed in Głuchowiec Quarry (Text-figs 8, 9) is probably related to the formation of strike-slip faults associated with development of the minor folds (cf. Konon 2015).

A local change from a transpressional to an extensional regime within the Chmielnik releasing stepover observed in Celiny Quarry resulted in reactivation of strike-slip faults as normal faults and the formation of subvertical permeability along the later faults that allowed for influx of external fluids. As a result I mode veins with large apertures were formed

(Text fig. 11A, C, D). Subsequent replacement of primary calcite and transition into secondary rhombohedral calcite towards the vein centres suggest that the calcite precipitated in an open space. The presence of secondary fabrics (Text-fig. 11C, D, G, H, I), within zones of altered primary calcite points to subsequent dissolution of the vein infilling that might have resulted from acidic fluids descending from the surface into the fault zones after the fault activity. We assume that this observation evidences the onset of a karst process within the fault zones in carbonate rocks and indicates a near-surface continental setting.

Interpretation of isotope and fluid inclusion data

The $\delta^{18}O$ values of vein-filling calcites are always negative (-7.4‰ on the average) and lower (by 3.5‰ on the average) than those of the corresponding limestones. Such ^{18}O depletion coupled with the low salinity of fluid inclusions in these calcites point to meteoric water as the main source of the parent fluids. The $\delta^{13}C$ values of the calcites are very similar (±0.8‰) to those of the corresponding limestones, which indicates that DIC in parent solutions was derived from the limestone dissolution. Tectonic stylolites, which occur frequently in all limestones studied, provide clear evidence of significant pressure-induced dissolution in these rocks related to continuous transpression. Hence, the DIC was liberated from the surrounding limestones to the fluids during the generation of tectonic stylolites, and calcite precipitated in the fault zones in a nearly closed system. This system was maintained by stress conditions during strike-slip faulting and enhanced by dilatant permeable structures developed within the fault zones.

Calcites from samples 64–66 represent an exception in the dataset. Although they also precipitated from meteoric water, their $\delta^{13}C$ values are much lower (almost by 12‰) than those of the corresponding limestones. Such depleted $\delta^{13}C$ values suggest that DIC in the parent fluids was at least partly derived from organic matter (OM), although some part of the DIC could be related to the dissolution of the surrounding limestones. The DIC liberated by the oxidation of OM is characterised by $\delta^{13}C$ values around -25‰ (Irwin *et al.* 1977), whereas that liberated from the dissolution of the surrounding limestone would have $\delta^{13}C$ values of +3‰ (Text-fig. 13). A simple mass balance calculation taking into account these two processes shows that about 60% of the DIC may have been produced by the former, and 40% by the latter process. The honey colour of these calcites from this locality indicates that organic matter may be present in the calcite. Indeed, organic particles are still preserved in some veins from this locality.

The co-occurrence of depleted $\delta^{13}C$ values and organic matter in calcites from normal faults with mode I veins from Celiny Quarry can be explained by open system conditions. The ^{13}C-depleted DIC could have been produced by the oxidation of OM in the surface soils and later transported by descending meteoric water deeper into the bedrock. The fluid inclusion study confirms meteoric vadose conditions for calcite precipitation in these veins. Consequently, the assembled data lead us to assume that the fault-related calcite veins formed in shallow superficial conditions, continental at the time of faulting.

A provisional model of fluid-rock interaction (Text-fig. 14) shows that two contrasting isotopic trends observed in the studied samples may be obtained from the same fluid, assuming different fluid/rock ratios. The trend subparallel to the $\delta^{18}O$ axis can be explained by a fluid/rock ratio lower or equal to 1, at a range of temperatures fluctuating between 50 and 200ºC as indicated by fluid inclusion data. The low fluid/rock ratio indicates a rock-buffered, closed fluid system. In contrast, the isotopic trend subparallel to the $\delta^{13}C$ axis, such as that observed in Celiny Quarry, indicates low temperature (~70ºC) alteration and precipitation of calcite at a fluid/rock ratio higher than 10, thus indicating an open, fluid-buffered system. Of course, other alternative models, overlapping the observed trends, could be calculated using different temperatures, fluid/rock ratios, chemical and isotope compositions of the parental fluid, but the trends observed in the Permo-Mesozoic cover of the Holy Cross Mountain Fold Belt are largely similar to other carbonate-hosted tectonic fluid systems (e.g., Kenis *et al*. 2000; Suchy *et al*. 2002; Slobodník *et al*. 2012).

Timing of strike-slip faulting in the south-western part of the Permo-Mesozoic cover of the HCFB

Two dominant stages of deformation can be distinguished within the Permo-Mesozoic cover of the HCFB: i) folding and ii) strike-slip faulting.

Late Cretaceous (Late Maastrichtian)–early Miocene (up to Langhian)

During the first stage of deformation, the main folds were created. The youngest folded rocks involved in the folds are of Late Cretaceous age (Cenomanian–Maastrichtian). This stage was followed by the second stage of deformation, in which

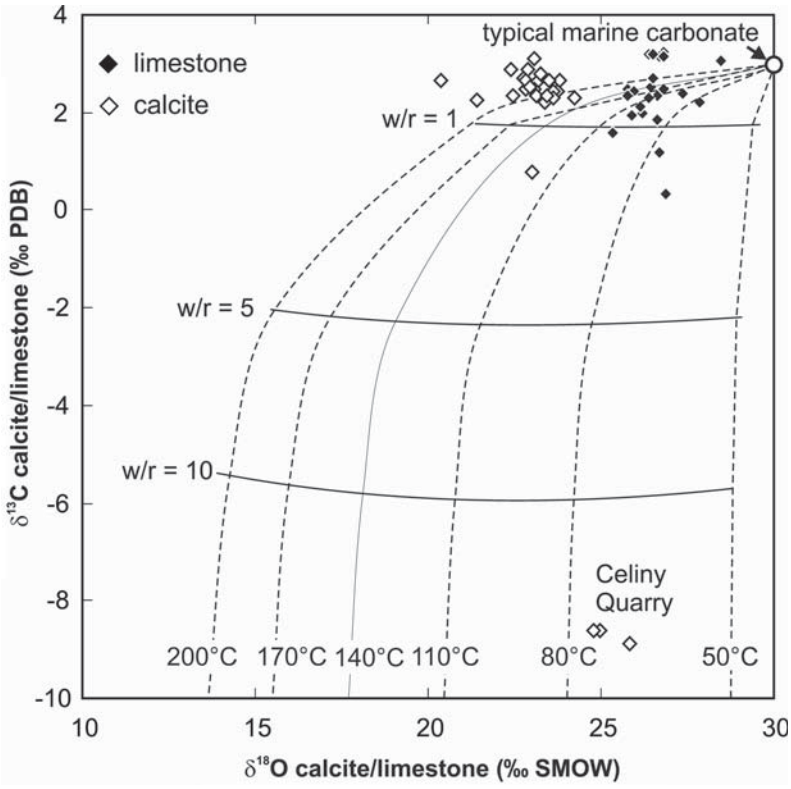

Text-fig. 14. Stable isotope composition of calcite veins and their host limestones superimposed onto fractionation curves calculated using a closed-system alteration model (Zheng 1993) with aqueous fluid containing 5 mol % of dissolved HCO_3^- with $\delta^{13}C$ = -25‰ (V-PDB), $\delta^{18}O$ = 3‰ (V-SMOW) and isotope fractionation factors from Zheng (1999) and Ohmoto and Rye (1979)

large-scale strike-slip faulting occurred, as a result of which the previously existing folds were cut by strike-slip faults (e.g., Text-figs 5A, 6B). The formation of the folds, as well as the activity of strike-slip faults in the Permo-Mesozoic cover was related to the late stage of inversion in the Polish Basin. An important constraint on the timing of the formation of strike-slip faults in the south-western part of the Permo-Mesozoic cover of the HCFB is related to observations of strike-slip faults and associated structures, such as the Mnin restraining stepover and the Chmielnik releasing stepover, which is overlain by younger Miocene rocks (Text-fig. 6A, C, D).

The occurrence of folds with a helicoidal geometry of the axial surfaces within the Mnin restraining stepover (Konon 2015; Konon *et al.* 2016) suggests that the stepover likely developed during/or after the late stage of folding after the Maastrichtian and before the Langhian (Text-figs 2A–C and 15) (Pożaryski 1964; Kutek and Głazek 1972; Dadlez *et al.* 1997; Konon *et al.* 2016). The change of the fold trends within the stepover suggests that the folds might have undergone modifications as a result of fault-associated dragging (Text-fig. 2C). Dragging of the beds resulted from the occurrence of a dextral strike-slip component along the Snochowice and Mieczyn-Lasocin main strike-slip faults bordering the stepover (Konon *et al.* 2016).

The timing of the deformation is consistent with the main uplift stage of the Holy Cross segment of the Polish Basin lasting, according to different authors, from the Turonian (Cenomanian?) up to the early Palaeogene (Krzywiec 2000, 2002, 2006, 2009; Resak *et al.* 2008; Krzywiec *et al.* 2009, 2018), from the Coniacian/Santonian up to early the Palaeogene (Dadlez and Marek 1997; Dadlez *et al.* 1998), or from the Maastrichtian up to the early Palaeogene (Kutek and Głazek 1972; Hakenberg and Świdrowska 1998, 2001; Świdrowska and Hakenberg 1999; Świdrowska 2007; Świdrowska *et al.* 2008). The time of uplift of this part of the Polish Basin is also consistent with deformation episodes recognised in the Inner Carpathians and the Pieniny Klippen Belt lasting from the Turonian up to the middle Miocene (Plašienka *et al.* 1997; Bada 1999; Text-fig. 15).

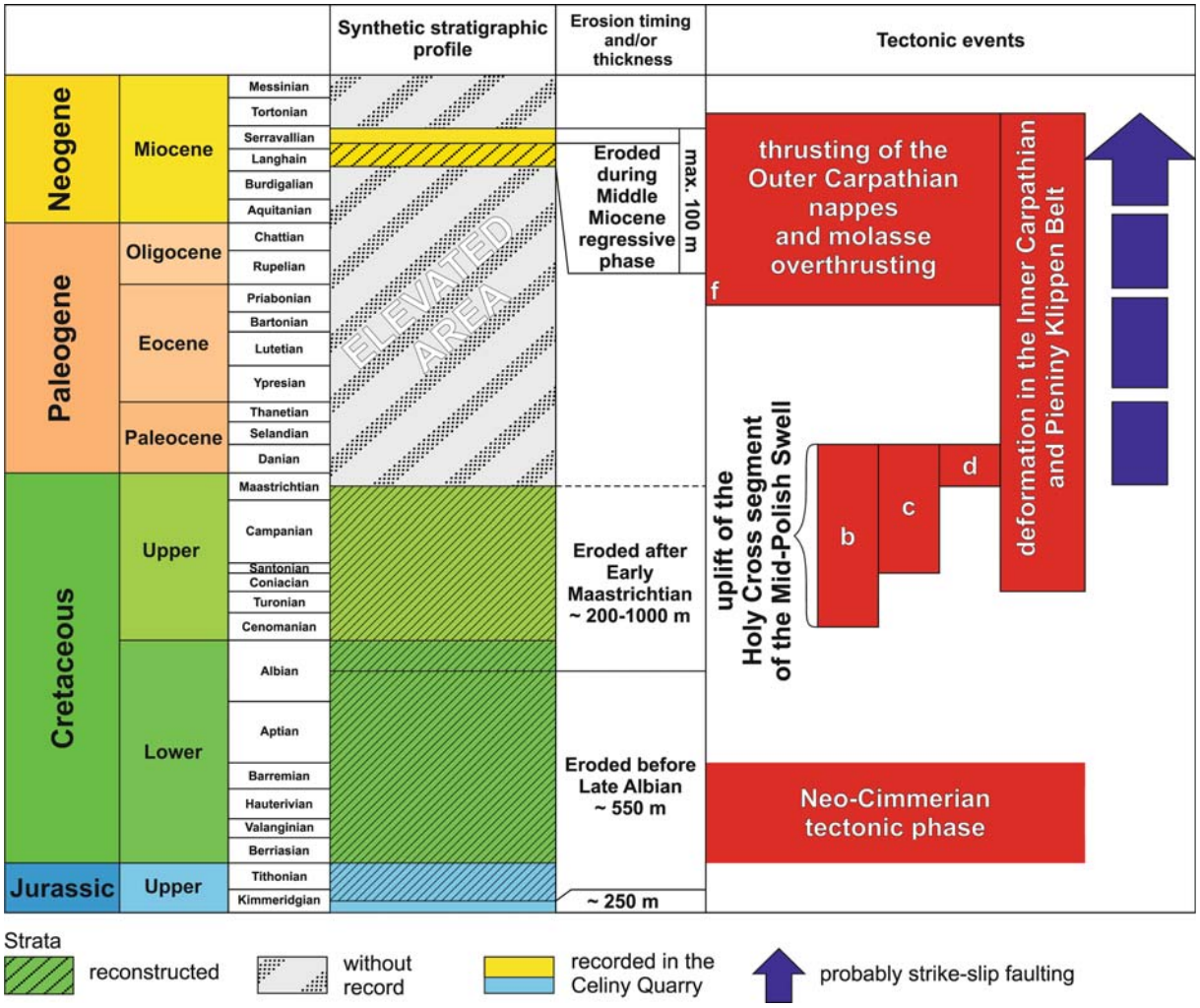

Text-fig. 15. Reconstruction of the Mesozoic and Cenozoic succession of the Celiny Quarry area (see text for details) and duration of the major regional structural episodes: Neo-Cimmerian movements: a) Late Jurassic/Early Cretaceous (Berriasian)–Aptian/Albian? (Masse *et al.* 1996; Golonka *et al.* 2003; Świdrowska *et al.* 2008); uplift of the Mid-Polish Swell; b) Turonian (Cenomanian?) – early Palaeogene (Krzywiec 2002, 2006, 2009; Resak *et al.* 2008; Krzywiec *et al.* 2009, 2018); c) Coniacian/Santonian – early Palaeogene (Dadlez and Marek 1997; Dadlez *et al.* 1998) Late Maastrichtian – early Palaeogene (Kutek and Głazek 1972; Hakenberg and Świdrowska 1998, 2001; Świdrowska and Hakenberg 1999; Świdrowska 2007; Świdrowska *et al.* 2008); deformation in the Inner Carpathians and Pieniny Klippen Belt: e) Turonian – middle Miocene (Plašienka *et al.* 1997; Bada 1999); deformation in the Outer Carpathians: f) Late Eocene – late Miocene (Kováč *et al.* 1993; Nemčok *et al.* 2006; Oszczypko 2006; Gągała *et al.* 2012; Krzywiec *et al.* 2014)

The Chmielnik releasing stepover formed from the Late Cretaceous (late Maastrichtian) up to the early Miocene (Langhian) (Text-figs 6B–D, 15). We propose that the activity of the strike-slip faults was related to a horizontal contraction, when the area was most probably uplifted and eroded (or no deposition took place) and only in the Early Badenian (Langhian) it was covered by a marine transgression (Radwański 1969; Text-fig. 6C).

Therefore, we assume that the episode of normal faulting recognised in the Chmielnik stepover was related to the extensional episode associated with the local activity of the releasing Chmielnik stepover or the uplift of the area.

Later deformations within the Carpathian orogen in Serravalian (Badenian/Sarmatian) time resulted in block movements, which together with the ongoing regression of the sea resulted in an increased erosion of Badenian and Sarmatian successions (Radwański 1973; Górka 2015). As a result of the

deformation, deposits of the 'detrital Sarmatian' were formed, which are observed in Celiny Quarry in direct contact with lower Kimmeridgian strata (e.g., Radwański 1969). Miocene sedimentation lasted till the Serravallian (Alexandrowicz *et al.* 1982; Piller *et al*. 2007; Stworzewicz *et al.* 2013; Hohenegger *et al.* 2014; Górka 2015).

Late Miocene (Tortonian)

Miocene rocks of Serravallian age in Celiny Quarry dissected by strike-slip faults suggest that the activity of strike-slip faults lasted at least up to the late Miocene (Tortonian) (Text-figs 4B and 6C). The stage of strike-slip faulting during the late Miocene in this part of the Permo-Mesozoic cover recognised also along the northern margin of the Carpathian Foredeep (e.g., Jarosiński 1992; Lamarche *et al*. 2002; Jarosiński *et al.* 2009) is consistent with the time of the latest thrusting movements of the Outer Carpathian fold-and-thrust belt in the contact zone with the Carpathian Foredeep Basin, which took place at ~10–11 Ma (Text-fig. 15) (Krzywiec *et al.* 2014).

CONCLUSIONS

Field observations, lithostratigraphic, microstructural and geochemical studies performed within exhumed shallow-generated damage zones of strike-slip faults dissecting the Permo-Mesozoic cover in the south-western part of the HCFB and Miocene rocks of the Carpathian Foredeep Basin have led to the following conclusions:

- The structural pattern of the strike-slip fault zones revealed the subsequent development of subsidiary faults and fractures, which were the main pathways for fluids that precipitated calcite during the fault activity.
- Calcite precipitated within fractures of modes: I, II, III and mixed modes related to displacement along the faults, and the mode I veins related to the extensional stage that terminated the fault activity in the Chmielnik region.
- Pressure dissolution of carbonate rocks acted during strike-slip faulting and its contribution was to provide the calcite that precipitated within dilational jogs and subsidiary faults and fractures within damage zones. This fluid-rock interaction was maintained by a transpressional regime.
- Calcite veins revealed two systems of fluid flow: i) a nearly closed, rock-buffered system related to strike-slip fault movement with $CaCO_3$ derived predominantly from the pressure dissolution of local carbonates and to a lesser extent from descending fluids of meteoric origin; and ii) an open system related to extensional activity of the releasing Chmielnik stepover or the uplift of the area, with a significant contribution of descending meteoric fluids that were conducted by permeable faults during and after their activity.
- The presence of fluids descending from the surface within fault-related calcite veins suggests that the map-scale strike-slip faulting might have taken place in a nonmarine, continental environment during Late Cretaceous, through Palaeogene to Langhian times.

Acknowledgments

This study was supported by Grant No. 2011/03/B/ST10/06341 of the Polish National Centre for Science "The role of strike-slip faulting during inversion of the south-western part of the Holy Cross segment of the Polish Basin". We thank Andrzej Żelaźniewicz and Jonas Kley for constructive comments that improved the manuscript. The early version of the manuscript greatly benefited from discussions with Bronisław Andrzej Matyja and Marcin Górka.

REFERENCES

Agosta, F. and Aydin, A. 2006. Architecture and deformation mechanism of a basin-bounding normal fault in Mesozoic platform carbonates, central Italy. *Journal of Structural Geology*, **28**, 1445–1467.

Agosta, F. and Kirschner, D.L. 2003. Fluid conduits in carbonate-hosted seismogenic normal faults of Central Italy. *Journal of Geophysical Research*, **108**, B4 2221, 1–13.

Ahlgren, S.G. 2001. The nucleation and evolution of Riedel shear zones as deformation bands in porous sandstone. *Journal of Structural Geology*, **23**, 1203–1214.

Alexandrowicz, S.W., Garlicki, A. and Rutkowski, J. 1982. Podstawowe jednostki litostratygraficzne miocenu zapadliska przedkarpackiego. *Kwartalnik Geologiczny*, **26**, 470–471.

Arndt, M., Virgo, S., Cox, S.F. and Urai, J.L. 2014. Changes in fluid patways in calcite vein mesh (Natih Formation, Oman Mountains): insights from stable isotopes. *Geofluids*, 1–28. DOI 10.1111/gfl.12083

Bada, G. 1999. Cenozoic stress field evolution in the Pannonian basin and surrounding orogens. Inferences from kinematic indicators and finite element modelling, 205 p. Vrije Universiteit Amsterdam, Amsterdam.

Bartlett, W.L., Friedman, M. and Logan, J.M. 1981 Experimen-

tal folding and faulting of rocks under confining pressure. *Tectonophysics*, **79**, 255–277.

Ben-Avraham, Z. 1985. Structural framework of the Gulf of Elat (Aqaba), northern Red Sea. *Journal of Geophysical Research*, **90**, 703–726.

Billi, A., Salvini, F. and Storti, F. 2003. The damage zone-fault core transition in carbonate rocks: implications for fault growth structure and permeability. *Journal of Structural Geology*, **25**, 1779–1794.

Bons, P.D., Elburg, M.A. and Gomez-Rivas, E. 2012. A review of the formation of tectonic veins and their microstructures. *Journal of Structural Geology*, **43**, 33–62.

Brogi, A. 2008. Fault zone architecture and permeability features in siliceous sedimentary rocks: Insights from the Rapolano geothermal area (Northern Apennines, Italy). *Journal of Structural Geology*, **30**, 237–256.

Caine, .JS., Evans, J.P. and Forster, C.B. 1996. Fault zone architecture and permeability structure. *Geology*, **24**, 1025–1028.

Caine, J.S. and Forster, C.B. 1999. Fault zone architecture and fluid flow; insights from field data and numerical modelling. In: Haneberg, W.C., Mozley, P.S., Moore, J.C. and Goodwin, L.B. (Eds), Faults and Sub-surface Fluid Flow in the Shallow Crust. *AGU Geophysical Monograph*, **113**, 101–127.

Caine, J.S., Bruhn, R.L. and Forster, C.B. 2010. Internal structure fault rocks and inferences regarding deformation fluid flow and mineralization in the seismogenic Stillwater normal fault, Dixie Valley Nevada. *Journal of Structural Geology*, **32**, 1576–1589.

Cao, S. and Neubauer, F. 2016. Deep crustal expressions of exhumed strike-slip fault systems: Shear zone initiation on rheological boundaries. *Earth-Science Reviews*, **162**, 155–176.

Chester, F.M. and Logan, J.M. 1986. Implications for mechanical-properties of brittle faults from observations of the Punchbowl fault zone, California. *Pure Applied Geophysics*, **124**, 79–106.

Chester, F.M., Evans, J.P. and Biegel, R.L. 1993. Internal structure and weakening mechanism of the S.Andreas Fault. *Journal of Geophysical Research*, **98**, 771–786.

Cieśla, E. and Lindner, L. 1990. Geological Map of Poland. Końskie sheet, scale 1:50 000. Wydawnictwa Geologiczne; Warszawa.

Cohen, K., Finney, S., Gibbard, P. and Fan, J.-X. 2013. The ICS international chronostratigraphic chart. *Episodes*, **36**, 199–204.

Cox, S.F. 2007. Structural and isotopic constraints on fluid flow regimes and fluid pathways during upper crustal deformation: An example from the Taemas area of the Lachlan Orogen, SE Australia. *Journal of Geophysical Research*, **112**, B08208, 1–23.

Crider, J.G. and Peacock, D.C.P. 2004. Initiation of brittle faults in the upper crust: A review of field observations. *Journal of Structural Geology*, **26**, 691–707.

Czarnocki, J. 1938. Carte geologique generale de la Pologne, feuille 4, Kielce, scale 1:100 000. Edition du Service Geologique de Pologne; Warszawa.

Czarnocki, J. 1961. Materiały do przeglądowej mapy geologicznej Polski. Region Świętokrzyski. Arkusz Kielce, scale 1:100 000. Wydanie B zaktualizowane. Wydawnictwa Geologiczne; Warszawa.

Dadlez, R. and Marek, S. 1997. Tektonika kompleksu permsko-mezozoicznego. *Prace Państwowego Instytutu Geologicznego*, **153**, 410–415.

Dadlez, R., Marek, S. and Pokorski, J. 1998. Atlas paleogeograficzny epikontynentalnego permu i mezozoiku w Polsce. Wydawnictwo Kartograficzne Polskiej Agencji Ekologicznej; Warszawa.

Dadlez, R. 2003. Mesozoic thickness pattern in the Mid-Polish Trough. *Geological Quarterly*, **47**, 223–240.

Dadlez, R., Jóźwiak, W. and Młynarski, S. 1997. Subsidence and inversion in the western part of Polish basin – data from aseismic velocities. *Geological Quarterly*, **41**, 197–208.

Doblas, M., Manecha, V., Hoyos, M. and Lopez-Ruiz, J. 1997. Slickenside and fault surface kinematic indicators on active normal faults of the Alpine Betic Cordilleras, Granada, southern Spain. *Journal of Structural Geology*, **19**, 159–170.

Durney, D.W. and Ramsay, J.G. 1973. Incremental strains measured by syntectonic crystal growths. In: De Jong, K.A. and Scholten, K. (Eds), Gravity and Tectonics, pp. 67–96. John Wiley & Sons; New York.

Ebner, M., Piazolo, S., Renard, F. and Koehn, D. 2010. Stylolite interfaces and surrounding matrix material: Nature and role of heterogeneities in roughness and microstructural development. *Journal of Structural Geology*, **32**, 1070–1084.

Engelder, T. 1999. Transitional-tensile fracture propagation: a status report. *Journal of Structural Geology*, **21**, 1049–1055.

Faulkner, D.R., Jackson, C.A.L., Lunn, R.J., Schlische, R.W., Shipton, Z.K., Wibberley, C.A.J. and Withjack, M.O. 2010. A review of recent developments concerning the structure mechanics and fluid flow properties of fault zones. *Journal of Structural Geology*, **32**, 1557–1575.

Faulkner, D.R., Lewis, A.C. and Rutter, E.H. 2003. On internal structure and mechanics of large strike-slip fault zones: field observations of the Carboneras fault in southern Spain. *Tectonophysics*, **367**, 235–251.

Filonowicz, P. 1967. Geological Map of Poland, Morawica sheet, scale 1:50 000. Wydawnictwa Geologiczne; Warszawa.

Filonowicz, P. and Lindner, L. 1986. Geological Map of Poland, Piekoszów sheet, scale 1:50 000. Wydawnictwa Geologiczne; Warszawa.

Finzi, Y., Hearn, E.H., Ben-Zion, Y. and Lyakhovsky, V. 2009. Structural properties and deformation patterns of evolving strike-slip faults: Numerical simulations incorporating damage rheology. *Pure Applied Geophysics*, **166**, 1537–1573.

Fitz-Diaz, E., Hudleston, P., Sebenaller, L., Kirschner, D., Camprubí, A., Tolson, G. and Puig, P.T. 2011. Insights into fluid flow and water-rock interaction during deformation of carbonate sequences in the Mexican fold-thrust belt. *Journal of Structural Geology*, **33**, 1237–1253.

Gągała, Ł., Vergés, J., Saura, E., Malata, T., Ringenbach, J.-C., Werner, P. and Krzywiec, P. 2012. Architecture and orogenic evolution of the northeastern Outer Carpathians from cross-section balancing and forward modeling. *Tectonophysics*, **532**, 223–241.

Golonka, J., Krobicki, M., Oszczypko, N., Ślączka, A. and Słomka, T. 2003. Geodynamic evolution and palaeogeography of the Polish Carpathians and adjacent areas during Neo-Cimmerian and preceding events (latest Triassic–earliest Cretaceous). *Geological Society Special Publications*, **208**, 137–158.

Golonka, J., Oszczypko, N. and Ślączka, A. 2000. Late Carboniferous–Neogene geodynamic evolution and palaeogeography of the circum-Carpathian region and adjacent areas. *Annales Societatis Geologorum Poloniae*, **70**, 107–136.

Górka, M.J. 2015. Kenozoiczna ewolucja świętokrzyskiego brzegu Paratetydy. Geologia wschodniego Ponidzia. In: Skompski, S. (Ed.), Ekstensja i inwersja powaryscyjskich basenów sedymentacyjnych. LXXXIV Zjazd Naukowy Polskiego Towarzystwa Geologicznego Chęciny, 9–11 września 2015 r., Sesja terenowa II, 138–144. Państwowy Instytut Geologiczny, Państwowy Instytut Badawczy; Warszawa.

Gradziński, M., Duliński, M., Hercman, H., Górny, A. and Przybyszowski, S. 2012. Peculiar calcite speleothems filling fissures in calcareous sandstones and their palaeohydrological and palaeoclimatic significance: an example from the Polish Carpathians. *Geological Quarterly*, **56**, 711–732.

Gratier, J.P., Dysthe, D. and Renard, F. 2013. The Role of Pressure Solution Creep in the Ductility of the Earth's Upper Crust. *Advances in Geophysics*, **54**, 47–179.

Gratier, J.-P., Favreau, P. and Renard, F. 2003. Modelling fluid transfer along California faults when integrating pressure solution crack sealing and compaction processes. *Journal of Geophysical Research*, **108 (B2)**, 28–52.

Gratier, J.-P., Frery, E., Deschamps, P., Røyne, A., Renard, F., Dysthe, D., Ellouz-Zimmerman, N. and Hamelin, B. 2009. How travertine veins grow from top to bottom and lift the rocks above them: The effect of crystallization force. *Geology*, **40**, 1015–1018.

Gratier, J.P., Richard, J., Renard, F., Mittempergher, S., Doan, M.L., Di Toro, G., Hadizadeh, J. and Boullier, A.M. 2011. Aseismic sliding of active faults by pressure solution creep: Evidence from the San Andreas Fault Observatory at Depth. *Geology*, **39**, 1131–1134.

Gruszczyński, M. and Mastella, L. 1986. Calcareous tufas in the area of the Mszana Dolna tectonic window. *Annales Societatis Geologorum Poloniae*, 56, 117–131. [In Polish with English summary]

Grzybowski, K. and Kutek, J. 1967. Geological Map of Poland, Lubień sheet, scale 1:50 000. Wydawnictwa Geologiczne; Warszawa.

Gutowski, J. and Koyi, H. 2007. Influence of oblique basement strike-slip faults on the Mesozoic evolution of the south-eastern segment of the Mid-Polish Trough. *Basin Research*, **19**, 67–86.

Hakenberg, M. 1969. Albian and Cenomanian between Małogoszcz and Staniewice, SW border of the Holy Cross Mountains. *Studia Geologica Polonica*, 26, 1–126. [In Polish with English summary]

Hakenberg, M. 1973. Geological Map of Poland, Chęciny sheet, scale 1:50 000. Wydawnictwa Geologiczne; Warszawa.

Hakenberg, M. and Świdrowska J., 2001. Cretaceous basin evolution in the Lublin area along the Teisseyre-Tornquist Zone (SE Poland). *Annales Societatis Geologorum Poloniae*, **71**, 1–20.

Hakenberg, M. and Świdrowska, J. 1998. Rozwój południowowschodniego segmentu bruzdy polskiej i jego związek ze strefami uskoków ograniczających (od permu do późnej jury). *Przegląd Geologiczny*, **46**, 503.

Hancock, P.L., Chalmers, R.M.L., Altunel, E. and Çakir, Z. 1999. Travitonics: using travertines in active fault studies. *Journal of Structural Geology*, **21**, 903–916.

Heap, M.J., Baud, P., Reuschlé, T. and Meredith, P.G. 2014. Stylolites in limestones: Barriers to fluid flow? *Geology*, **42**, 51–54.

Heap, M.J., Reuschlé, T., Baud, P., Renard, F. and Iezzi, G. 2018. The permeability of stylolite-bearing limestone. *Journal of Structural Geology*, **116**, 81–93.

Hohenegger, J., Ćorić, S. and Wagreich, M. 2014. Timing of the middle miocene Badenian stage of the central Paratethys. *Geologica Carpathica*, **65**, 55–66.

Irwin, H., Curtis, C., and Coleman, M. 1977. Isotopic evidence for source of diagenetic carbonates formed during burial of organic-rich sediments. *Nature*, **269**, 209–213.

Janiec, J. 1991. Geological Map of Poland. Żarnów sheet, scale 1:50 000. Wydawnictwa Geologiczne; Warszawa.

Jarosiński, M. 1992. The tectonics of the argillaceous rocks of the cover of the sulphur deposit in Machow near Tarnobrzeg in the light of the mesostructural analysis. *Geological Quarterly*, **36**, 121–150. [In Polish with English summary]

Jarosiński, M., Poprawa, P. and Ziegler, P.A. 2009. Cenozoic dynamic evolution of the Polish Platform. *Geological Quarterly*, **53**, 3–26.

Jurkiewicz, I. 1961. Materiały do przeglądowej mapy geologicznej Polski. Region Świętokrzyski, arkusz Przedbórz. Wydanie B zaktualizowane, skala 1:100,000. Wydawnictwa Geologiczne; Warszawa.

Jurkiewicz, I. 1965. Geological Map of Poland, Czermno sheet, scale 1:50 000. Wydawnictwa Geologiczne; Warszawa.

Jurkiewicz, I. 1967. Geological Map of Poland, Radoszyce sheet, scale 1:50 000. Wydawnictwa Geologiczne; Warszawa.

Kenis, I., Muchez, P.H., Sintubin, M., Mansy, J.L. and Lacquement, F. 2000. The use of a combined structural, stable isotope and fluid inclusion study to constrain the kinematic history at the northern Variscan front zone (Bettrechies, northern France). *Journal of Structural Geology*, **22**, 589–602.

Kim, S.T., Mucci, A. and Taylor, B.E. 2007. Phosphoric acid fractionation factors for calcite and aragonite between 25 and 75°C: Revisited. *Chemical Geology*, **246**, 135–146.

Kim, Y.-S. and Sanderson, D.J. 2010. Inferred fluid flow through fault damage zones based on the observation of stalactites in carbonate caves. *Journal of Structural Geology*, **32**, 1305–1316.

Kim, Y.-S., Peacock, D.C.P. and Sanderson, D.J. 2003. Strike-slip faults and damage zones at Marsalforn, Gozo Island, Malta. *Journal of Structural Geology*, **25**, 793–812.

Knipe, R.J. 1993. The influence of fault zone processes and diagenesis on fluid flow. In: Horbury, A.D. and Robinson, A. (Eds), Diagenesis and Basin Development. *Association of Petroleum Geologists Studies in Geology*, **36**, 35–51.

Koehn, D., Renard, F., Toussaint, R. and Passchier, C.W. 2007. Growth of stylolite teeth patterns depending on normal stress and finite compaction. *Earth and Planetary Letters*, **257**, 582–595.

Konon, A. 2007. Strike-slip faulting in the Kielce Unit, Holy Cross Mountains, central Poland. *Acta Geologica Polonica*, **57**, 415–441.

Konon, A. 2015. Przejawy przesuwczości w obrębie południowo-zachodniego obrzeżenia permsko-mezozoicznego Gór Świętokrzyskich. LXXXIV Zjazd Naukowy Polskiego Towarzystwa Geologicznego, Chęciny, 9–11 września 2015, Ekstensja i inwersja powaryscyjskich basenów sedymentacyjnych, pp. 59–67. Państwowy Instytut Geologiczny, Państwowy Instytut Badawczy; Warszawa

Konon, A., Ostrowski, S., Rybak-Ostrowska, B., Ludwiniak, M., Śmigielski, M., Wyglądała, M., Uroda, J., Kowalczyk, S., Mieszkowski, R. and Kłopotowska, A. 2016. Mnin restraining stepover – evidence of significant Cretaceous–Cenozoic dextral strike-slip faulting along the Teisseyre-Tornquist Zone? *Acta Geologica Polonica*, **66**, 435–455.

Konon. A and Mastella, L. 2001. Structural evolution of the Gnieździska Syncline – regional implications for the SW Mesozoic Margin of the Holy Cross Mountains (Central Poland). *Annales Societatis Geologorum Poloniae*, **71**, 189–199.

Kováč, M., Nagymarosy, A., Soták, J. and Šutovská, K. 1993. Late Tertiary paleogeographic evolution of the Western Carpathians. *Tectonophysics*, **226**, 401–415.

Krajewski, R. 1961. Materiały do Przeglądowej mapy geologicznej Polski. Region Świętokrzyski, arkusz Końskie, skala 1:100 000. Wydanie B zaktualizowane. Wydawnictwa Geologiczne; Warszawa.

Krzywiec, P. 2000. O mechanizmach inwersji bruzdy środkowopolskiej – wyniki interpretacji danych sejsmicznych. *Biuletyn Państwowego Instytutu Geologicznego*, **393**, 135–166.

Krzywiec, P. 2002. Mid-Polish Trough inversion – seismic examples, main mechanisms and its relationship to the Alpine-Carpathian collision. *EGU Stephan Mueller Special Publication Series*, **1**, 151–165.

Krzywiec, P. 2006. Structural inversion of the Pomeranian and Kuiavian segments of the Mid-Polish Trough-lateral variations in timing and structural style. *Geological Quarterly*, **50**, 151–168.

Krzywiec, P. 2007. Tectonics of the Lublin area (SE Poland) – new views based on results of seismic data interpretation. *Biuletyn Państwowego Instytutu Geologicznego*, **422**, 1–18. [In Polish]

Krzywiec, P. 2009. Devonian–Cretaceous repeated subsidence and uplift along the Teisseyre-Tornquist zone in SE Poland—Insight from seismic data interpretation. *Tectonophysics*, **475**, 142–159.

Krzywiec, P., Gutowski, J., Walaszczyk, I., Wróbel, G. and Wybraniec, S. 2009. Tectonostratygraphic model of the Late Cretaceous inversion along the Nowe Miasto-Zawichost fault zone, SE Mid-Polish Trough. *Geological Quarterly*, **53**, 27–48.

Krzywiec, P., Oszczypko, N., Bukowski, K., Oszczypko-Clowes, M., Śmigielski, M., Stuart, F.M., Persano, C. and Sinclair, H.D. 2014. Structure and evolution of the Carpathian thrust front between Tarnów and Pilzno (Pogórska Wola area, southern Poland) – results of integrated analysis of seismic and well data. *Geological Quarterly*, **58**, 409–426.

Krzywiec, P., Stachowska, A. and Stypa, A. 2018. The only way is up-on Mesozoic uplifts and basin inversion events in SE Poland. *Geological Society, London, Special Publications*, **469**, SP469-14.

Kuleta, M. and Zbroja, S. 2006. Wczesny etap rozwoju pokrywy permsko-mezozoicznej w Górach Świętokrzyskich. In: Skompski, S. and Żylińska, A. (Eds), 77 Zjazd Naukowy Polskiego Towarzystwa Geologicznego, Ameliówka k. Kielc, 28–30 czerwca 2006 r., Materiały konferencyjne, pp. 105–125. Państwowy Instytut Geologiczny; Warszawa.

Kutek, J. and Głazek, J. 1972. The Holy Cross area, central Poland, in the Alpine cycle. *Acta Geologica Polonica*, **22**, 603–651.

Kutek, J. 1968. The Kimmeridgian and Uppermost Oxfordian in the SW margin of the Holy Cross Mts, Central Poland. Part I. Stratigraphy. *Acta Geologica Polonica*, **18**, 493–586. [In Polish with English summary]

Kwapisz, B. 1983. Geological Map of Poland, Przedbórz sheet, scale 1:50 000. Wydawnictwa Geologiczne; Warszawa.

Labaume, P., Carrio-Schaffhauser, E., Gamond, J.F. and Renard, F. 2004. Deformation mechanism and fluid-driven

mass transfers in the recent fault zones of the Corinth Rift (Greece). *Comptes Rendus Geoscience*, **336**, 375–383.

Lamarche, J., Bergerat, F., Lewandowski, M., Mansy, J.L., Świdrowska, J. and Wieczorek, J. 2002. Variscan to Alpine heterogeneous paleo-stress field above a major Palaeozoic suture in the Carpathian for eland (siuth-eastern Poland). *Tectonophysics*, **357**, 55–80.

Leszczyński, K. 1998. Lower Cretaceous (excluding Lower Berriasian and Upper Albian) – thickness. In: Dadlez, R., Marek, S. and Pokorski, J. (Eds), Palaeographical Atlas of the Epicontinental Permian and Mesozoic in Poland (1:2 500 000), plate 64. Polish Geological Institute; Warszawa. [in Polish with English summary]

Łyczewska, J. 1971. Geological map of Poland, Busko Zdrój sheet (917), scale 1:50 000. Wydawnictwa Geologiczne; Warszawa.

Marcinowski, R. and Radwański, A. 1983. The Mid-Cretaceous transgression onto the Central Polish Uplands (marginal part of the Central European Basin). *Zitteliana*, **10**, 65–95.

Marek, S. 1988. Palaeothickness, lithofacies and palaeotectonics of the epicontinental Lower Cretaceous in Poland. *Geological Quarterly*, **32**, 157–176.

Marshak, S., Geise, P.A., Alvarez, W. and Engelder, T. 1982. Mesoscopic fault array of the northern Umbrian Apennine fold belt, Italy: Geometry of conjugate shear by pressure-solution slip. *Geological Society of America Bulletin*, **93**, 1013–1022.

Masse, J.-P., Philip, J. and Camoin, G. 1995. The Cretaceous Tethys. In: Nairn, A.E.M., Ricou, L.C., Vrielynck, B. and Dercourt, J. (Eds), The Tethys Ocean, pp. 215–236. Springer; New York.

Mastella, L. and Rybak-Ostrowska, B. 2012. Tectonic control of tufa occurrences in the Podhale Synclinorium (Central Western Carpathians, southern Poland). *Geological Quarterly*, **56**, 733–744.

Mastella, L. 1988. Budowa i ewolucja strukturalna okna tektonicznego Mszany Dolnej, polskie Karpaty Zewnętrzne. *Annales Societatis Geologorum Poloniae*, **58**, 53–173.

Mastella, L. and Konon, A. 2002. Non-planar strike-slip Gnieździska-Brzeziny fault (SW Mesozoic margin of the Holy Cross Mountains central Poland). *Acta Geologica Polonica*, **52**, 471–480.

Matyja, B.A. 1977. The Oxfordian in the south-western margin of the Holy Cross Mts. *Acta Geologica Polonica*, **27**, 41–64.

Matyja, B.A. 2009. Development of the Mid-Polish Trough versus Late Jurassic evolution in the Carpathian Foredeep area. *Geological Quarterly*, **53**, 49–62.

Matyja, B.A. 2012. Mezozoik. In: Skompski, S. (Ed.), Góry Świętokrzyskie. 25 najważniejszych odsłonięć geologicznych, pp. 17–23. Uniwersytet Warszawski, Wydział Geologii; Warszawa.

Matyja, B.A., Wierzbowski, A. and Drewniak, A. 1996. Węglanowe osady basenu późnojurajskiego zachodniego obrzeżenia Gór Świętokrzyskich. In: Karnkowski, P.H. (Ed.), Analiza basenów sedymentacyjnych a nowoczesna sedymentologia. Materiały konferencyjne V Krajowego Spotkania Sedymentologicznego, A1-16. Warszawa.

Mazur, S., Krzywiec, P. and Scheck-Wenderoth, M. 2005. Different modes of Late Cretaceous–Early Tertiary inversion in the North German and Polish Basin. *International Journal of Earth Sciences*, **94**, 782–798.

Micklethwaite, S. and Cox, S.F. 2004. Fault-segment rupture, aftershock-zone fluid flow, and mineralization. *Geology*, **32**, 813–816.

Nemčok, M., Krzywiec, P., Wojtaszek, M., Ludhová, L., Kleckler, R.A., Sercombe, W.J. and Coward, M.P. 2006. Tertiary development of the Polish and eastern Slovak parts of the Carpathian accretionary wedge: insights from balanced cross-sections. *Geologica Carpathica*, **57**, 355–370.

Nuriel, P., Weinberger, R., Rosenbaum, G., Golding, S.D., Zhao, J., Uysal, I.T., Bar-Matthews, M. and Gross, M.R. 2012. Timing and mechanism of late-Pleistocene calcite vein formation across the Dead Sea Fault Zone, northern Israel. *Journal of Structural Geology*, **36**, 43–54.

Ohmoto, H. and Rye, R.O. 1979. Isotope of sulfur and carbon. In: Barnes, H.L. (Ed.), Geochemistry of Hydrothermal Deposits, pp. 509–567. John Wiley & Sons; New York.

Oliver, N.H.S. 1996. Review and classification of structural controls on fluid flow during regional metamorphism. *Journal of Metamorphic Geology*, **14**, 477–492.

Oszczypko, N. 2006. Late Jurassic–Miocene evolution of the Outer Carpathian fold-and-thrust belt and its foredeep basin (Western Carpathians, Poland). *Geological Quarterly*, **50**, 169–194.

Passchier, C.W. and Trouw, R.A.J. 1996. Microtectonics, 289 p. Springer Verlag; Berlin.

Petit, J.P. 1987. Criteria for the sense of movement on fault surfaces in brittle rocks. *Journal of Structural Geology*, **9**, 597–608.

Pieńkowski, G. 2004. The epicontinental Lower Jurassic of Poland. *Polish Geological Institute Special Papers*, **12**, 1–154.

Pieńkowski, G.1991. Eustatically-controlled sedimentation in the Hettangian–Sinemurian (Early Jurassic) of Pland and Sweden. *Sedimentology*, **38**, 503–518.

Pili, É., Poitrsson, F. and Gratier, J-P. 2002. Carbon-oxygen isotope and trace element constraints on how fluids percolate faulted limestones from the San Andreas Fault system: partitioning of fluid sources and pathways. *Chemical Geology*, **190**, 231–250.

Piller, W.E., Harzhauser, M. and Mandic, O. 2007. Miocene Central Paratethys stratigraphy-current status and future directions. *Stratigraphy*, **4**, 151–168.

Plašienka, D., Grecula, P., Putiš, M., Kováč, M. and Hovorka, D. 1997. Evolution and structure of the Western Carpathians: an overview. In: Grecula, P., Hovorka, D. and Kováč,

M. (eds), Geological Evolution of the Western Carpathians, pp. 1–24. Geocomplex; Bratislava.

Pollard, D.D. and Segall, P. 1987. Theoretical displacements stresses near fractures in rocks: with applications to faults, joints, veins, dikes, and solution surfaces. In: Atkinson, B.K. (Ed.), Fracture Mechanics of Rocks, pp. 277–349. Academic Press; London.

Pożaryski, W. 1964. Outline of Palaeozoic and Mesozoic tectonics of the Polish Lowland. *Kwartalnik Geologiczny*, **8**, 1–41. [In Polish with English summary]

Radwański, A. 1969. Lower Tortonian transgression onto the southern slopes of the Holy Cross Mts. *Acta Geologica Polonica*, **19**, 1–164. [In Polish with English summary]

Radwański, A. 1973. Lower Tortonian transgression onto the south-eastern and eastern slopes of the Holy Cross Mts. *Acta Geologica Polonica*, **23**, 375–434. [In Polish with English summary]

Radwański, A. and Górka, M. 2012. Wybrzeże morza mioceńskiego – Korytnica, Lubania i głazowisko klifowe w Skotnikach. In: Skompski, S. (Ed.), Góry Świętokrzyskie. 25 najważniejszych odsłonięć geologicznych, pp. 131–137. Uniwersytet Warszawski, Wydział Geologii; Warszawa.

Ramsay, J.G. 1980. The crack-seal mechanism of rock deformation. *Nature*, **284**, 135–139.

Ramsay, J.M. and Chester, F.M. 2004. Hybrid fracture and the transition from extension fracture to shear fracture. *Nature*, **428**, 63–66.

Reading, H.G. 1980. Characteristics and recognition of strike-slip fault systems. In: Balance, P.F. (Ed.), Sedimentation in Oblique-slip Mobile Zones. *Special Publications, International Association of Sedimentologists*, **4**, 7–26.

Resak, M., Narkiewicz, M. and Littke, R. 2008. New basin modelling results from the Polish part of the Central European Basin system: implications for the Late Cretaceous–Early Paleogene structural inversion. *International Journal of Earth Sciences*, **97**, 955–972.

Riedel, W. 1929. Zur Mechanik Geologischer Brucherscheinungen. *Zentral-blatt fur Mineralogie, Geologie und Paleontologie B*, 354–368.

Romanek, A. 1982. Geological Map of Poland, Chmielnik sheet (885), scale 1:50 000. Wydawnictwa Geologiczne; Warszawa.

Rosenbaum, J. and Sheppard, S.M. 1986. An isotopic study of siderites, dolomites and ankerites at high temperatures. *Geochimica Cosmochimica Acta*, **50**, 1147–1150.

Różycki, S.Z. 1961. Materiały do przeglądowej mapy geologicznej Polski. Region Świętokrzyski, arkusz Włoszczowa. Wydanie B zaktualizowane, skala 1:100 000. Wydawnictwa Geologiczne; Warszawa.

Rybak-Ostrowska, B., Konon, A., Domonik, A., Uroda, J. and Poszytek, A. 2017. Shallow generated damage within non-planar strike-slip fault zones – role of the sedimentary rocks in the slip accommodation, SW Holy Cross Mountains, Poland. *International Journal of Earth Sciences (Geologische Rundschau)*, **106**, 1863–1888.

Scholz, Ch.H. 2002. The Mechanics of Erthquakes and Faulting, 467 p. Cambridge University Press; Cambridge.

Schreurs, G. 1994. Experiments on strike-slip faulting and block rotation. *Geology*, **22**, 567–570.

Schreurs, G. 2003. Fault development and interaction in distributed strike-slip shear zones: an experimental approach. In: Storti, F., Holdswoth, R.E. and Salvini, F. (Eds), Intraplate Strike-slip Deformation Belts. *Geological Society, London, Special Publications*, **210**, 35–52.

Segall, P. and Pollard, D.D. 1980. Mechanics of Discontinuous Faults. *Journal of Geophysical Research*, **85**, 4337–4350.

Senkowicz, E. 1955. Geological map of Poland, Pińczów sheet (884), scale 1:50 000. Wydawnictwa Geologiczne; Warszawa.

Senkowiczowa, H. 1961. The Röth and Muschelkalk on the southern slope of the Święty Krzyż Mts. between Czarna Nida and Chmielnik. *Biuletyn Instytutu Geologicznego*, **167**, 41–89. [In Polish with English summary]

Sibson, R.H. 1996. Structural permeability of fluid-driven fault-fracture meshes. *Journal of Structural Geology*, **18**, 1031–1042.

Sibson, R.H. 2000. Fluid involvement in normal faulting. *Journal of Geodynamics*, **29**, 469–499.

Slobodník, M., Melichar and R., Hurai, V., Bakker, R.J. 2012. Litho-stratigraphic effect on Variscan fluid flow within the Prague synform, Barrandain: Evidence based on C, O, Sr isotopes and fluid inclusions. *Marine and Petroleum Geology*, **35**, 128–138.

Stworzewicz, E., Prisyazhnyuk, V.A. and Górka, M. 2013. Systematic and palaeoecological study of Miocene terrestrial gastropods from Zwierzyniec (southern Poland). *Annales Societatis Geologorum Poloniae*, **83**, 179–200.

Suchy, V., Dobes, P., Filip, J., Stejskal, M. and Zeman, A. 2002. Conditions for veining in the Barrandian Basin (Lower Palaeozoic), Czech Republic: evidence from fluid inclusions and apatite fission track analysis. *Tectonophysics*, **348**, 25–50.

Świdrowska, J. 2007. Kreda w regionie lubelskim-sedymentacja i jej tektoniczne uwarunkowania. *Biuletyn Państwowego Instytutu Geologicznego*, **422**, 63–77.

Świdrowska, J. and Hakenberg, M. 1999. Subsydencja i początki inwersji bruzdy śródpolskiej na podstawie analizy map miąższości i litofacji osadów górnokredowych. *Przegląd Geologiczny*, **47**, 61–68.

Świdrowska, J., Hakenberg, M., Poluhtovič, B., Seghedi, A. and Višnâkov, I. 2008. Evolution of the Mosozoic Bains on the southwestern edge of the East European Craton (Poland, Ukraine, Moldova, Romania). *Studia Geologica Polonica*, **130**, 3–130.

Sylvester, A.G. 1988. Strike slip faults. *Geological Society of America Bulletin*, **100**, 1666–1703.

Szajn, J. 1977. Geological Map of Poland, Nagłowice sheet, scale 1:50 000. Wydawnictwa Geologiczne; Warszawa.

Szajn, J. 1980. Geological Map of Poland, Włoszczowa sheet, scale 1:50,000. Wydawnictwa Geologiczne; Warszawa.

Szajn, J. 1983. Geological Map of Poland, Oleszno sheet, scale 1:50 000. Wydawnictwa Geologiczne; Warszawa.

Uysal, I.T., Fenga, Y., Zhao, J., Altunel, E., Weatherley, D., Karabacak, V., Cengizd, O., Golding, S.D., Lawrence, M.G. and Collerson, K.D. 2007. U-series dating and geochemical tracing of late Quaternary travertine in co-seismic fissures. *Earth and Planetary Science*, **257**, 450–462.

Wakabayashi, J. 2007. Stepovers that migrate with respect to affected deposits: field characteristics and speculation on some details of their evolution. In: Cunningham, W.D. and Mann, P. (Eds), Tectonics of Strike-Slip Restraining and Releasing Bends. *Geological Society, London, Special Publications*, **290**, 169–188.

Wakabayashi, J., Hengesh, J.V. and Sawyer, T.L. 2004. Four-dimensional transform fault processes: progressive evolution of step-overs and bends. *Tectonophysics*, **392**, 279–301.

Walczowski, A. 1973. Geological map of Poland, Stopnica sheet (918), scale 1:50 000. Wydawnictwa Geologiczne; Warszawa.

Wibberley, C.J.A. and Shimamoto, T. 2003. Internal structure and permeability of major strike-slip fault zones: the Median Tectonic Line in Mie Prefecture, Southwest Japan. *Journal of Structural Geology*, **25**, 59–78.

Wiberley, C.A.J., Yielding, G. and Di Toro, G. 2008. Recent advances in the understanding of fault zone internal structure: a review. *Geological Society, London, Special Publications*, **299**, 5–33.

Woodcock, N.H. and Schubert, C. 1994. Continental strike-slip tectonics. In: Hancock, P.L. (Ed.), Continental Deformation, 251–263. Pergamon Press; New York.

Zhang, Y., Schaubs, P.M., Zhao, C., Ord, A., Hobbs, B. and Barnicoat, A.C. 2008. Fault-related dilation, permeability enhancement, fluid flow and mineral precipitation patterns: numerical models. In: Wibberley, C.A.J., Kurz, W., Imber, J., Holdsworth, R.E. and Collettini, C. (Eds), The internal Structure of Fault Zones. *Geological Society, London, Special Publications*, **299**, 239–255.

Zheng, Y.F. 1999. Oxygen isotope fractionation in carbonate and sulfate minerals. *Geochemical Journal*, **33**, 109–126.

Zheng, Y.F. and Hoefs, J. 1993. Carbon and oxygen isotopic covariations in hydrothermal calcites. Theoretical modeling on mixing processes and application to Pb-Zn deposits in the Harz Mountains, Germany. *Mineralium Deposita*, **28**, 79–89.

Ziegler, P.A. 1982. Geological Atlas of Western and Central Europe. 130 p. Elsevier; Amsterdam.

Ziegler, P.A. 1987. Late Cretaceous and Cenozoic intra-plate compressional deformations in the Alpine foreland – a geodynamic model. *Tectonophysics*, **137**, 389–420.

Ziegler, P.A. 1990a. Collision related intra-plate compression deformations in Western and Central Europe. *Journal of Geodynamics*, **11**, 357–388.

Ziegler, P.A. 1990b. Geological Atlas of Western and Central Europe (2nd edition). 239 p. Shell Internationale Petroleum Mij. BV and Geological Society; London.

Manuscript submitted: 11th January 2019
Revised version accepted: 7th September 2019